

Electroweak phase transition in singlet extensions of the standard model with dimension-six operators

V. K. Oikonomou^{1,2} and Apostolos Giovanakis¹

¹*Department of Physics, Aristotle University of Thessaloniki, Thessaloniki 54124, Greece*

²*L.N. Gumilyov Eurasian National University, Astana, 010008, Kazakhstan*

 (Received 28 December 2023; accepted 2 March 2024; published 26 March 2024)

The significance of the electroweak phase transition is undeniable, and although initially it was believed that it was second order, it is now believed that it is a first-order transition. However, it is not a strong first-order phase transition in the context of the standard model, and the remedy to this issue is to use the Higgs portal and directly couple the Higgs to a hidden scalar sector. This can result in a strong electroweak phase transition, while the couplings to a hidden scalar are constrained by several phenomenological constraints, such as the sphaleron rate criterion and the branching ratio of the Higgs to invisible channels. In this work, we consider the standard singlet extensions of the standard model, including dimension-six non-renormalizable operators that couple a real singlet scalar field with the Higgs doublet. As a result, we examine the effects of those Higgs-singlet couplings on the electroweak phase transition. The effective theory, where the nonrenormalizable couplings originate from, is considered to be active beyond 15 TeV. As we show, the Universe experiences a two-step electroweak phase transition, a primary phase transition in the singlet sector at a high temperature, and then a subsequent first-order phase transition from the singlet vacuum to the electroweak vacuum. The singlet's phase transition can either be second order or first order, depending on the singlet mass and its couplings to the Higgs. In particular, we show that the dimension-six operator assists in generating a strong electroweak phase transition in regions of the parameter space that were excluded in the previous singlet extensions of the standard model. This is further apparent for low singlet masses $m_S < m_H/2$, which are rarely taken into account in the literature due to the invisible branching ratio of the Higgs boson. In some limited cases in the parameter space, the electroweak phase transition is weakened by the presence of the higher order operator.

DOI: [10.1103/PhysRevD.109.055044](https://doi.org/10.1103/PhysRevD.109.055044)

I. INTRODUCTION

The most mysterious eras of our Universe are the primordial eras, specifically the inflationary era and the reheating era. These two eras are strongly related, and to date, no direct evidence of the occurrence of these two exists. Much light on these two mysterious eras is expected to be shed by the upcoming stage 4 Cosmic Microwave Background (CMB) experiments [1,2] and of course by the future interferometric gravitational wave experiments, like the LISA, BBO, DECIGO, and the Einstein telescope [3–11]. The stage 4 CMB experiments will directly probe the B modes of the CMB polarization, if they exist, and the interferometers will probe the stochastic primordial gravitational waves. The latter is already confirmed to exist

at nanohertz frequencies, in 2023 by the NANOGrav collaboration [12] and by the EPTA [13], the PPTA [14], and the CPTA [15] Collaborations. The future seems to be fruitful in this research line.

Moreover, due to the complete absence of particle detections at the LHC since the detection of the Higgs particle, and recall that the LHC functions at a center-of-mass energy 13.6 TeV, modern high energy physics relies on gravitational wave experiments and astrophysical observations in order to address fundamental problems related to baryogenesis, electroweak phase transition, and dark matter. However, we must mention that the particles colliding at the LHC are basically hadrons, so have some non-negligible form factors, so the actual theories and energies probed at the LHC might actually correspond to lower energies than 13.6 TeV center of mass. To date, the electroweak phase transition is believed to be a first-order phase transition [16], although earlier studies indicated that it was a second-order phase transition [17]. The order of the electroweak phase transition has triggered a great deal of heated debate in the last decades. In the past years, it was

Published by the American Physical Society under the terms of the Creative Commons Attribution 4.0 International license. Further distribution of this work must maintain attribution to the author(s) and the published article's title, journal citation, and DOI. Funded by SCOAP³.

shown in numerous studies using perturbative calculations that the electroweak phase transition is a first-order phase transition [16]. On the other hand, it is understood that this topic is still controversial. In fact, recent simulations and studies indicate that with the Higgs mass being ~ 125 GeV, the phase transition is even a crossover, and not a first-order phase transition, in the customary sense; see, for example, [18,19], and for an older lattice simulation, see [17], which points out to a second-order phase transition. A first-order phase transition would provide nonequilibrium conditions, and thus, one of the Sakharov criteria [20] would hold true and the baryogenesis could occur during the electroweak phase transition. First-order phase transitions also produce a stochastic gravitational wave background and are thus observationally important [11,21–44]. The problem with the electroweak phase transition in the standard model (SM) is that it is not strong enough, and thus, singlet extensions of the SM active through the Higgs portal have been proposed to solve it [25,28,42–70]. In this work, we consider the standard real singlet extension, including higher order non-renormalizable interactions between the Higgs field and a real singlet scalar field, and we concretely examine the effects of these Higgs-singlet couplings on the electroweak phase transition. The dimension-six non-renormalizable operators are considered to originate from a weakly coupled effective theory that remains active well beyond 15 TeV. As we demonstrate, the Universe experiences two phase transitions, a primary phase transition in the singlet scalar sector at high temperatures, and then the ordinary electroweak phase transition. The singlet scalar phase transition can either be a second-order or a first-order phase transition, which depends solely on the singlet scalar mass and its couplings to the Higgs boson. More importantly, we demonstrate that due to the presence of the dimension-six non-renormalizable operator, the electroweak phase transition is stronger in some regions of the parameter space, which were excluded in the standard singlet extensions of the SM without the higher order operators. However, we show that, in some limited cases for some parameter values, the electroweak phase transition is actually weakened by the presence of the higher order operator.

This paper is organized as follows: In Sec. II, we present the effective potential for the SM enriched with the singlet extension, including the higher order non-renormalizable operators. In Sec. III, we discuss the constraints from the electroweak baryogenesis, which must be taken into account in our analysis; in Secs. IV and V, we showcase the allowed parameter space of our model, and we also discuss various phenomenological constraints and constraints from invisible Higgs decay. Finally, in Sec. VI, we study and present all the different possibilities for the electroweak phase transition in our singlet-extended SM, and the conclusions follow at the end of the article.

II. SM EFFECTIVE POTENTIAL WITH SINGLET EXTENSIONS AND HIGHER ORDER OPERATORS

We extend the SM by introducing a real singlet scalar field ϕ [25,28,42–70] equipped with a \mathbb{Z}_2 discrete symmetry, under which $\phi \rightarrow -\phi$ and all other SM fields remain unaffected. In addition, we shall assume that a higher-dimensional operator of the singlet scalar field is weakly coupled to the Higgs sector. This dimension-six higher order non-renormalizable operator originates from an effective theory active at a scale M , which will be assumed to be way higher than the electroweak scale, of the order $M = 15\text{--}100$ TeV, a fact that is further motivated by the lack of new particle observations in the LHC, beyond the electroweak symmetry breaking scale [25]. The dimensionless coupling λ is the Wilson coefficient of the higher order effective theory, and we shall assume that the theory is strongly coupled. In general, the coefficient of the higher order term is considered small such that $\lambda/M^2 < 10^{-4}$ GeV $^{-2}$, and the contribution of the higher-dimensional operator to the invisible Higgs decays is omitted. The tree-level potential for the doublet Higgs field and the singlet scalar field is given by

$$V_0(H, \phi) = -\mu_H^2 |H|^2 + \lambda_H |H|^4 - \frac{\mu_S^2}{2} \phi^2 + \frac{\lambda_S}{4} \phi^4 + \lambda_{HS} |H|^2 \phi^2 + \frac{\lambda}{M^2} |H|^2 \phi^4, \quad (1)$$

where $m_H = \sqrt{2}\mu_H$ is the Higgs boson mass, $\lambda_H > 0$ is the Higgs self-coupling, and λ_{HS} is the Higgs-singlet interaction coupling, which is assumed to be positive. In this work, we consider one of the simplest higher-dimensional operators in the real singlet extensions to the standard model. The $D > 6$ operators are suppressed, and it can be easily shown that their effect on the electroweak phase transition is not so strong for valid values of the Wilson coefficients. In principle, dimension-eight and higher order operators can be added due to some non-perturbative physics motivated Lagrangian terms of the form $\sim |H|^2 \cos(\frac{\phi}{M})$, but the dominant term is always the dimension-six operator. The tree-level potential of the singlet scalar field is determined by the four parameters μ_S , λ_S , λ_{HS} , and λ and the energy scale M . The SM Higgs doublet is parametrized as follows:

$$H = \frac{1}{\sqrt{2}} \begin{pmatrix} \chi_1 + i\chi_2 \\ h + i\chi_3 \end{pmatrix}, \quad (2)$$

where h is the Higgs boson, χ_1, χ_2, χ_3 are three Goldstone bosons, and $v = \mu_H/\sqrt{\lambda_H}$ is the electroweak symmetry breaking minimum of the Higgs scalar field h at zero

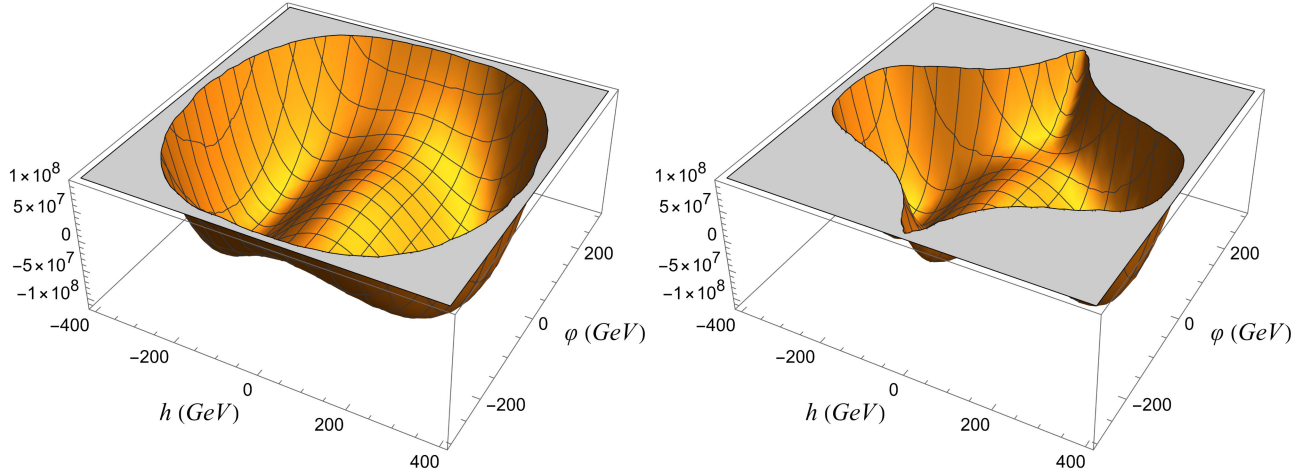


FIG. 1. The tree-level potential in the field space for $\lambda = 0$ (left) and $\lambda/M^2 = 2 \times 10^{-5} \text{ GeV}^{-2}$ (right), where the global minimum is the electroweak vacuum. We assumed that $m_S = 62.5 \text{ GeV}$, $\lambda_{\text{HS}} = 0.1$, and $a = 0.1$.

temperature, without the singlet sector. The tree-level potential (1) in the unitary gauge takes the following form:

$$V_0(h, \phi) = -\frac{\mu_H^2}{2}h^2 + \frac{\lambda_H}{4}h^4 - \frac{\mu_S^2}{2}\phi^2 + \frac{\lambda_S}{4}\phi^4 + \frac{\lambda_{\text{HS}}}{2}h^2\phi^2 + \frac{\lambda}{2M^2}h^2\phi^4, \quad (3)$$

which is shown in Fig. 1. In the context of the SM, we consider only the dominant contributions in the one-loop finite temperature effective potential coming from the gauge bosons, the top quark (the heaviest fermion), the Higgs and Goldstone bosons. The effective masses of the Higgs boson, the singlet scalar field, and those fields that are coupled to the background fields h and ϕ are

$$m_h^2(h, \phi) = -\mu_H^2 + 3\lambda_H h^2 + \lambda_{\text{HS}}\phi^2 + \frac{\lambda}{M^2}\phi^4, \quad (4)$$

$$m_\chi^2(h, \phi) = -\mu_H^2 + \lambda_H h^2 + \lambda_{\text{HS}}\phi^2 + \frac{\lambda}{M^2}\phi^4, \quad (5)$$

$$m_S^2(h, \phi) = -\mu_S^2 + 3\lambda_S\phi^2 + \lambda_{\text{HS}}h^2 + \frac{6\lambda}{M^2}h^2\phi^2, \quad (6)$$

$$m_W^2(h) = \frac{g^2}{4}h^2, \quad (7)$$

$$m_Z^2(h) = \frac{g^2 + g'^2}{4}h^2, \quad (8)$$

$$m_t^2(h) = \frac{y_t^2}{2}h^2, \quad (9)$$

where g, g' and y_t are the $SU(2)_L$, $U(1)_Y$ and top quark Yukawa couplings, respectively, and $m_t = 173 \text{ GeV}$,

$m_W = 80.4 \text{ GeV}$, $m_Z = 91.2 \text{ GeV}$, and $m_t = 173 \text{ GeV}$ at the current vacuum state of the Universe ($h = v$).

The full effective potential is defined as the sum of the tree-level potential and the one-loop finite-temperature effective potential, which splits into a zero-temperature and a temperature-dependent part, which will be presented explicitly in the next two sections.

A. Zero temperature corrections

The zero-temperature one-loop contribution to the effective potential is called the Coleman-Weinberg (CW) potential [71] and is computed as the sum of all one-particle irreducible Feynman diagrams with zero external momenta and a single loop. In the $\overline{\text{MS}}$ renormalization scheme, it is written as

$$V_1^i(h, \phi) = (-1)^{F_i} n_i \frac{m_i^4(h, \phi)}{64\pi^2} \left[\ln \left(\frac{m_i^2(h, \phi)}{\mu_R^2} \right) - C_i \right], \quad (10)$$

where $i = \{h, \chi, \phi, W, Z, t\}$ counts the particles that mainly contribute to the CW potential and couple with the Higgs doublet and the singlet scalar field, $F_i = 1$ (0) for fermions (bosons), n_i is the number of degrees of freedom of each particle i , μ_R denotes the renormalization scale, and $C_i = 3/2$ (5/6) for scalars and fermions (gauge bosons). The degrees of freedom of each particle i are

$$\begin{aligned} n_h &= 1, & n_\chi &= 3, & n_\phi &= 1, \\ n_W &= 6, & n_Z &= 3, & n_t &= 12. \end{aligned} \quad (11)$$

The choice of the renormalization scale leads to an uncertainty in the critical temperature T_c and to other related quantities [66,72–74]. Different schemes can be followed to compute the CW potential and handle this uncertainty, such as the on-shell (OS) and on-shell-like

schemes (OS-like). In the literature, the OS-like scheme is commonly adopted since it has a fixed prescription for the renormalization scales for each particle, and the tree-level relations among the parameters are valid at higher loop corrections, like in the OS scheme. For instance, in this scheme, the CW potential takes the form,

$$V_1^{(\text{OS})}(h, \phi) = \sum_i \frac{(-1)^{F_i} n_i}{64\pi^2} \left[m_i^4(h, \phi) \left(\ln \frac{m_i^2(h, \phi)}{m_i^2(v, 0)} - \frac{3}{2} \right) + 2m_i^2(h, \phi)m_i^2(v, 0) \right]. \quad (12)$$

However, both OS schemes suffer from an infrared divergence that originates from the Goldstone bosons as they acquire a zero mass at zero temperature. This subtlety can be rectified by the proposed methods in Refs. [75,76], but in our study, we extensively work in the $\overline{\text{MS}}$ scheme.

In Ref. [66], it was concluded that varying μ_R from $m_t/2$ to $2m_t$, the OS-like and $\overline{\text{MS}}$ schemes agreed with each other within the scale uncertainties, which were (3.8–6.2)%

in the critical temperature T_c and (10–23)% in the ratio v_c/T_c . In the case of $\mu_R = m_t/2$, the two results were approximately identical with the highest accuracy. In our study, we have chosen $\mu_R = m_t/2$. A similar analysis was also developed in Ref. [72]. Lastly, the renormalization scale dependence could be eliminated by the renormalization group equations (RGE) improvement for the CW potential [77–81], but this approach is left to be implemented in future studies.

B. Finite temperature corrections to the effective potential

The temperature dependence of the finite-temperature one-loop potential is interpreted in terms of the free energy of an ideal gas. The effective potential at finite temperature contains the effective potential at zero temperature, which was presented in the previous section. Thus, we focus on its temperature-dependent component¹ for each particle i , and it is equal to

$$V_T^i(h, \phi, T) = (-1)^{F_i} \frac{n_i T^4}{2\pi^2} \int_0^\infty dx x^2 \ln \left[1 - (-1)^{F_i} \exp \left(-\sqrt{x^2 + \frac{m_i^2(h, \phi)}{T^2}} \right) \right], \quad (13)$$

where the thermal functions integrals are defined as follows:

$$J_{B/F}(y^2) = \int_0^\infty dx x^2 \ln \left[1 \mp \exp \left(-\sqrt{x^2 + y^2} \right) \right], \quad (14)$$

where the subscript B (F) stands for bosons (fermions). The thermal functions can be computed numerically, but they also admit a high-temperature expansion (for $|y^2| \ll 1$) [81], which will be applied in this work and is given by

$$J_B(y^2) = -\frac{\pi^4}{45} + \frac{\pi^2}{12} y^2 - \frac{\pi^3}{6} y^3 - \frac{1}{32} y^4 \log \left(\frac{y^2}{a_b} \right) + O(y^6), \quad (15)$$

$$J_F(y^2) = -\frac{7\pi^4}{360} - \frac{\pi^2}{12} y^2 - \frac{1}{32} y^4 \log \left(\frac{y^2}{a_f} \right) + O(y^6), \quad (16)$$

where $a_b = \pi^2 \exp(3/2 - 2\gamma_E)$, $a_f = 16\pi^2 \exp(3/2 - 2\gamma_E)$, ζ denotes the Riemann ζ -function, and γ_E is the Euler-Mascheroni constant. Numerical analysis shows that the high-temperature expansion up to the logarithmic term is accurate to better than 5% for $y \leq 1.6$ for fermions and

$y \leq 2.2$ for bosons [82,83]. Moreover, this approximation for both the potential and its derivatives also agrees with the exact form to better than approximately 10% for the values $y \lesssim (1-3)$, depending on the function [84].

The symmetry restoration at high temperature implies that conventional perturbation theory breaks down near the critical temperature [81]. As a matter of fact, if perturbation theory were to remain valid, considering the temperature independence of the tree-level potential, temperature-dependent radiative corrections should be incapable of restoring the symmetry. In particular, it can be proved that the one-loop approximation in terms of small coupling constants breaks down at a high temperature due to the appearance of infrared divergences for the zero Matsubara modes of bosonic degrees of freedom [40]. Therefore, higher loop corrections that are contained in the daisy diagrams have to be resummed in the perturbative expansion. In principle, the so-called daisy resummation is a method aiming to sum all powers of the coupling constant resulting in a theory where the effective mass is $m_i^2 \rightarrow M_i^2 = m_i^2 + \Pi_i(T)$, which is called the thermal mass, and $\Pi_i(T)$ is the temperature-dependent self-energy corresponding to the one-loop resummed diagrams to leading powers of the temperature. This replacement in

¹This component vanishes at zero temperature.

the full temperature-dependent effective potential is usually described by the Parwani scheme [85] and leads to

$$V_{\text{eff}}(h, \phi, T) = V_0(h, \phi) + \sum_i [V_1^i(m_i^2(h, \phi) + \Pi_i(T)) + V_T^i(m_i^2(h, \phi) + \Pi_i(T), T)]. \quad (17)$$

A similar method, developed by Arnold and Espinosa [86], resums only the zero Matsubara modes that cause the infrared divergence. In the Arnold-Espinosa scheme, the resummed full effective potential is written as follows:

$$V_{\text{eff}}(h, \phi, T) = V_0(h, \phi) + \sum_i [V_1^i(m_i^2(h, \phi)) + V_T^i(m_i^2(h, \phi), T) + V_{\text{ring}}^i(m_i^2(h, \phi), T)] \quad (18)$$

The last term is added to the field dependent masses,² and it is given by

$$V_{\text{ring}}^i(m_i^2(h, \phi), T) = \frac{\bar{n}_i T}{12\pi} [m_i^3(h, \phi) - (m_i^2(h, \phi) + \Pi_i(T))^{3/2}] \quad (19)$$

for the particles $i = \{h, \chi, \phi, W, Z, \gamma\}$ and $\bar{n}_i = \{1, 3, 1, 2, 1, 1\}$ is the modified number of degrees of freedom, which takes into account that only the longitudinal polarizations of the gauge bosons contribute to the temperature-dependent self-energy [16,86]. A comparison between these schemes is presented in Refs. [72,73], where it is

$$M_{\text{GB}}^2(h, T) = \begin{pmatrix} \frac{1}{4}g^2h^2 + \frac{11}{6}g^2T^2 & 0 & 0 & 0 \\ 0 & \frac{1}{4}g^2h^2 + \frac{11}{6}g^2T^2 & 0 & 0 \\ 0 & 0 & \frac{1}{4}g^2h^2 + \frac{11}{6}g^2T^2 & -\frac{1}{4}gg'h^2 \\ 0 & 0 & -\frac{1}{4}gg'h^2 & \frac{1}{4}g^2h^2 + \frac{11}{6}g^2T^2 \end{pmatrix}. \quad (25)$$

Nevertheless, the photon and the Z boson are not mass eigenstates at high temperature since there is an additional mixing term between the Z boson and the photon [73]. Therefore, the gauge boson mass matrix has the following eigenvalues for the longitudinal photon and Z boson:

$$M_{Z_L}^2 = \frac{1}{2} \left[\frac{1}{4}(g^2 + g'^2)h^2 + \frac{11}{6}(g^2 + g'^2)T^2 + \sqrt{(g^2 - g'^2)^2 \left(\frac{1}{4}h^2 + \frac{11}{6}T^2 \right)^2 + \frac{g^2g'^2}{4}h^4} \right], \quad (26)$$

²This scheme is equivalent to the Parwani scheme in the high-temperature limit [84].

apparently shown that the numerical differences between the two schemes regarding the critical temperature and the ratio v_c/T_c are relatively small. Finally, the Arnold-Espinosa scheme is widely preferred in beyond the standard model physics, and it will be adopted throughout this paper.

In this model, the temperature-dependent self-energy for the scalar fields are computed as

$$\Pi_h(T) = \Pi_\chi(T) = \left(\frac{3g^2}{16} + \frac{g^2}{16} + \frac{y_t^2}{4} + \frac{\lambda_H}{2} + \frac{\lambda_{\text{HS}}}{12} \right) T^2, \quad (20)$$

$$\Pi_S(T) = \left(\frac{\lambda_S}{4} + \frac{\lambda_{\text{HS}}}{3} + \frac{\lambda v^2}{2M^2} \right) T^2. \quad (21)$$

The thermal corrections of the gauge bosons require special treatment as the transverse gauge fields have zero thermal corrections [16]. According to Ref. [16], we compute the temperature-dependent self-energy of the longitudinal gauge bosons in the high-temperature limit,

$$\Pi_{W_L}(T) = \frac{11}{6}g^2T^2, \quad (22)$$

$$\Pi_{Z_L}(h, T) = \frac{11}{6}g^2T^2 - \frac{g^2}{4}h^2, \quad (23)$$

$$\Pi_{\gamma_L}(h, T) = \frac{11}{6}g^2T^2 + \frac{g^2}{4}h^2, \quad (24)$$

where the gauge boson mass matrix in the basis $(A_\mu^1, A_\mu^2, A_\mu^3, B_\mu)$ is nondiagonal

$$M_{\gamma_L}^2 = \frac{1}{2} \left[\frac{1}{4}(g^2 + g'^2)h^2 + \frac{11}{6}(g^2 + g'^2)T^2 - \sqrt{(g^2 - g'^2)^2 \left(\frac{1}{4}h^2 + \frac{11}{6}T^2 \right)^2 + \frac{g^2g'^2}{4}h^4} \right]. \quad (27)$$

In the limit $m_W^2(h)/T^2 \ll 1$, the full resummed mass eigenvalues (26) and (27) can be effectively approximated by those in Eqs. (23) and (24). The numerical difference between these expressions is small, which indicates that one could treat the photon and Z boson as mass eigenstates [73].

Finally, it is essential to mention that the full effective potential can have imaginary contributions in the case of negative squared effective masses. This holds true especially for the scalar fields due to the logarithmic and cubic terms in the thermal functions (15) and (16) since the gauge bosons and the top quark have always a positive squared effective mass. In general, the effective mass in the logarithmic term is canceled by its counterpart in the one-loop zero-temperature correction. Moreover, the daisy resummation could potentially cure the imaginary part originating from the cubic term, which signals the

breakdown of the perturbative expansion.³ Nevertheless, the $m_i^2(h, \phi) + \Pi_i(T)$ in the ring correction can be negative for certain temperatures and field values. As a result, the effective potential is still complex, and we consider only the real part of the full effective potential and ensure the field's stability during the phase transition, provided its imaginary counterpart remains sufficiently insignificant. A relevant discussion can be found in Ref. [37].

To sum up, in the Arnold-Espinosa scheme, the full effective potential that describes the dynamics of the phase transition of our singlet-extended SM reads

$$V_{\text{eff}}(h, \phi, T) = -\frac{\mu_H^2}{2}h^2 + \frac{\lambda_H}{4}h^4 - \frac{\mu_S^2}{2}\phi^2 + \frac{\lambda_S}{4}\phi^4 + \frac{\lambda_{HS}}{2}h^2\phi^2 + \lambda\frac{h^2\phi^4}{2M^2} + \sum_i (-1)^{F_i} n_i \frac{m_i^4(h, \phi)}{64\pi^2} \left[\ln\left(\frac{m_i^2(h, \phi)}{\mu_R^2}\right) - C_i \right] \\ + \sum_i \frac{n_i T^4}{2\pi^2} J_B\left(\frac{m_i^2(h, \phi)}{T^2}\right) - 12\frac{T^4}{2\pi^2} J_F\left(\frac{m_i^2(h)}{T^2}\right) + \sum_i \frac{\bar{n}_i T}{12\pi} [m_i^3(h, \phi) - (M_i^2(h, \phi, T))^{3/2}], \quad (28)$$

where $i = \{h, \phi, \chi, W, Z, \gamma\}$ corresponds to the bosons in the extended SM.

Our main results are based on the high-temperature expansion (15) and (16), and its validity is primarily checked by the condition on the value of the ratio M_i/T , which was previously explained. If these conditions are violated, we numerically compute the full effective potential (28). Therefore, according to the high-temperature expansion, the full effective potential (28) becomes

$$V_{\text{eff}}^{\text{HT}}(h, \phi, T) = -\frac{\mu_H^2}{2}h^2 + \frac{\lambda_H}{4}h^4 - \frac{\mu_S^2}{2}\phi^2 + \frac{\lambda_S}{4}\phi^4 + \frac{\lambda_{HS}}{2}h^2\phi^2 + \frac{\lambda}{2M^2}h^2\phi^4 \\ \times \frac{m_h^2(h, \phi)}{24}T^2 - \frac{T}{12\pi} [M_h^2(h, \phi, T)]^{3/2} + \frac{m_h^4(h, \phi)}{64\pi^2} \left[\ln\left(\frac{a_b T^2}{\mu_R^2}\right) - \frac{3}{2} \right] \\ + \frac{3m_\chi^2(h, \phi)}{24}T^2 - \frac{3T}{12\pi} [M_\chi^2(h, \phi, T)]^{3/2} + \frac{3m_\chi^4(h, \phi)}{64\pi^2} \left[\ln\left(\frac{a_b T^2}{\mu_R^2}\right) - \frac{3}{2} \right] \\ + \frac{m_\phi^2(h, \phi)}{24}T^2 - \frac{T}{12\pi} [M_\phi^2(h, \phi, T)]^{3/2} + \frac{m_\phi^4(h, \phi)}{64\pi^2} \left[\ln\left(\frac{a_b T^2}{\mu_R^2}\right) - \frac{3}{2} \right] \\ + \frac{6m_W^2(h)}{24}T^2 - \frac{4T}{12\pi} m_W^3(h) - \frac{2T}{12\pi} [M_{W_L}^2(h, T)]^{3/2} + \frac{6m_W^4(h)}{64\pi^2} \left[\ln\left(\frac{a_b T^2}{\mu_R^2}\right) - \frac{5}{6} \right] \\ + \frac{3m_Z^2(h)}{24}T^2 - \frac{2T}{12\pi} m_Z^3(h) - \frac{T}{12\pi} [M_{Z_L}^2(h, T)]^{3/2} + \frac{3m_Z^4(h)}{64\pi^2} \left[\ln\left(\frac{a_b T^2}{\mu_R^2}\right) - \frac{5}{6} \right] \\ + \frac{12m_t^2(h)}{48}T^2 - \frac{12m_t^4(h)}{64\pi^2} \left[\ln\left(\frac{a_f T^2}{\mu_R^2}\right) - \frac{3}{2} \right] - \frac{T}{12\pi} [M_{\gamma_L}^2(h, T)]^{3/2}, \quad (29)$$

where the effective and thermal masses are given above. It is interesting to notice that only the cubic terms of the gauge bosons do not cancel each other in the high-temperature expansion of the effective potential and the ring corrections, in contrast with the rest of the fields that have the same degrees of freedom in the ring correction. Our main aim is to analyze in detail the phase transitions that occur at finite temperature for the effective potential (29). This is a cumbersome procedure though since the parameter space is highly constrained from various aspects, and several

limitations and constraints apply that reduce significantly the range of the values of the free parameters. Thus, before we actually study the phase transition, in the next few sections, we shall narrow down the values of the free parameters that are phenomenologically acceptable and comply with all the experimental and theoretical constraints.

³Weinberg and Wu claimed that the imaginary part of the effective potential could also be interpreted as a decay rate of a state of the scalar fields [87].

III. ELECTROWEAK BARYOGENESIS CONSTRAINTS

Initially, the vacuum of the Universe was stabilized at the origin $(h, \phi) = (0, 0)$. At a high temperature T_s , a phase transition starts in the ϕ direction from the origin to a nonzero vacuum expectation value (VEV). This phase transition can be either first or second order, depending on the singlet extension model's parameters. As the Universe cools down, a second local minimum appears in the full effective potential, where a barrier is gradually formed between the two local minima. At the temperature T_c , the electroweak phase transition occurs as a first-order phase transition when the two local minima $(0, v'_s)$ and $(v_c, 0)$ are degenerate as illustrated in Figs. 4 and 5. Therefore, the transition from the false vacuum to the true vacuum proceeds via thermal tunneling, when the bubbles of the broken phase nucleate within the surrounding plasma of the phase with the false vacuum.

The observed baryon asymmetry of the Universe can be attributed to the electroweak baryogenesis (EWBG). This is a physical mechanism in the early Universe that generates an asymmetry between baryons and antibaryons in the electroweak phase transition. This asymmetry is established if the so-called Sakharov criteria [20] are fulfilled, which namely are: (i) baryon number violation, (ii) C - CP violation, and (iii) departure from thermal equilibrium. The EWBG satisfies these criteria requiring a first-order phase transition [81, 88–90]. Baryon creation in EWBG occurs at the vicinity of the expanding bubble walls. More specifically, ahead of the bubble wall, CP and C asymmetries in particle number densities can be produced by CP -violating interactions of the plasma with the expanding bubble wall of the true vacuum [91]. Then, these asymmetries diffuse into the symmetric phase in front of the bubble wall, where they are converted to baryons by electroweak sphalerons [92]. In the broken phase, the rate of sphaleron transitions can be strongly suppressed to avoid washing out the generated baryons. Hence, it is necessary for a successful EWBG scenario that the baryon asymmetry generated at the expanding bubble wall is not washed out by sphalerons within the broken phase. In particular, EWBG requires a strong first-order electroweak phase transition, characterized by the following condition, which provides an approximation to a factor in the rate of sphaleron transitions in the broken phase,

$$\frac{v_c}{T_c} > 0.6 - 1.4. \quad (30)$$

The lower bound of this so-called sphaleron rate criterion⁴ varies between 0.6 and 1.4 due to some uncertainties in the

⁴This ratio does not respect gauge invariance, and special treatment is required to derive the gauge invariant form. However, this approach affects the numerical results much less than the two-loop approximation [93].

precise calculation, but it is conventionally taken to be one [93, 94]. In our study, we also consider the lower limit in this range for the sake of completeness. The critical temperature T_c and the Higgs VEV v_c are computed numerically in this paper.

In fact, the three Sakharov criteria are satisfied in the SM [81]: The baryon number is violated by nonperturbative effects, CP violation can be induced by the CKM phase in the fermion mass matrix, and the Universe is out of equilibrium due to the electroweak phase transition. However, CP violation is insufficient to produce large enough chiral asymmetries to explain the observed baryon-to-entropy ratio. Furthermore, the electroweak phase transition should be strong enough first order, a requirement that is not met by the SM as demonstrated in Appendix A; thus, the motivation for singlet extensions is clear. These drawbacks in the SM motivate beyond the standard model physics, which should suggest an extension of the Higgs potential to realize a strong first-order electroweak phase transition and an extra source of CP violation. The former is successfully achieved by singlet scalar extensions of SM, two-Higgs doublet models, and higher order operators to SM [44], and this occurs in our case, too.

CP -violating sources in EWBG can be obtained by a plethora of models such as real and complex singlet scalar extensions [49, 95–98], two-Higgs doublet models [99], and composite Higgs models [100]. A promising CP -violating source could be a dimension-six operator, which is introduced as an effective field theory [49]. This extension couples the singlet with the top quark's mass considering the singlet particle as a dark matter candidate and modifying top quark's mass for nonzero values of the singlet scalar field so that it is given by

$$y_t \bar{Q}_L H \left(1 + \frac{\eta}{\Lambda^2} \phi^2 \right) t_R + \text{H.c.} \quad (31)$$

where η is the complex phase, and Λ is the energy scale of the effective field theory. Consequently, the top quark acquires a complex phase that varies in space along the profile of the bubble wall, offering the crucial source of CP violation needed to explain baryon asymmetry.

This higher dimension operator does not affect the critical temperature and VEVs as it vanishes at both the Higgs and singlet direction. This operator mostly raises the height of the barrier at temperature T_c , which leads to a thinner bubble wall. It is additionally assumed that ϕ/Λ remains very small, resulting in a negligible contribution to the effective potential, which does not significantly affect the dynamics of the phase transition, and it is not included in our analysis of the effective potential; see also [49, 95]. However, a reasonable claim could be that the fact that this higher dimension operator does not affect the critical temperature and VEVs since it vanishes at both the Higgs and singlet direction could lead to a deeper minimum away

from these points. This could be possible, but it is clearly mentioned that the ratio ϕ/Λ remains very small, resulting in a negligible contribution to the effective potential, and a deeper minimum cannot be generated in the context of a valid perturbative analysis. The aforementioned higher dimension operator is further discussed in [49]. The choice of the phase η is not restricted by any additional experimental constraints due to the forbidden Higgs-singlet mixing and the behavior of the singlet at high temperatures. As a result, this phase can be chosen to be maximally CP violating, and it easily generates sufficient baryon asymmetry for EWBG [49]. However, potential loop contributions to electric dipole moments might exist. This is an important aspect that we did not take into account in this work to simplify the discussion. The two-loop Barr-Zee contributions to the electric dipole moments are discussed in [100]. However, this would require Higgs-singlet mixing, which is not the case in our model. In that scenario CP would be broken spontaneously at high temperature.

IV. ALLOWED PARAMETER SPACE FOR THE MODEL AND PHENOMENOLOGICAL CONSTRAINTS

The parameter space of the model is generally described by the three parameters of the real singlet extension μ_S , λ_S , and λ_{HS} , and the Wilson coefficient⁵ λ . In addition, a strong EWPT can be realized by a parameter space that is mainly restricted by the sphaleron rate criterion, the vacuum structure, the values of couplings, and on the fact whether these values break perturbation theory, and the invisible Higgs decay width.

Firstly, we proceed on the premise that the current vacuum state of the Universe is described by the Higgs VEV at zero temperature with broken $SU(2) \times U(1)_Y$ symmetry, while the singlet has a zero VEV with unbroken \mathbb{Z}_2 symmetry. As a result, we demand that the Higgs minimum is the global minimum of the effective potential at zero temperature by requiring

$$V_0(v, 0) < V_0(0, v_s) \Rightarrow \lambda_S > \lambda_H \frac{\mu_S^4}{\mu_H^4}, \quad (32)$$

where v_s is the zero-temperature VEV of the singlet scalar field in the ϕ direction, and it is assumed that $\mu_S^2 > 0$ for a two-step electroweak phase transition.⁶ We additionally demand that the tree-level potential is bounded from below, which leads to $\lambda_S > 0$ and $\lambda > 0$. Also the condition (32) is essential to ensure that the electroweak vacuum is the global minimum of the effective potential at zero temperature, and the parameter values we shall use ensure that the electroweak vacuum is always the lowest minimum of

the effective potential. This vacuum structure further implies that the singlet scalar field acquires the following mass squared at zero temperature, which is required to be positive,

$$m_S^2 = -\mu_S^2 + \lambda_{HS} v^2 > 0. \quad (33)$$

An expression for the minimum value of λ_S can then be derived by Eqs. (32) and (33), and it is

$$\lambda_S^{\min} = \frac{\lambda_H}{\mu_H^4} (m_S^2 - \lambda_{HS} v^2)^2. \quad (34)$$

Accordingly, the quartic coupling can be cast into the form,

$$\lambda_S = \lambda_S^{\min} + a, \quad (35)$$

where a is a positive parameter.⁷ Consequently, it is more convenient and suitable to study the parameter space in terms of m_S , λ_{HS} , and λ for a given parameter a . However, it is worth mentioning that Eq. (32) could be rewritten in the equivalent form in terms of the other parameters,

$$\mu_S^2 < v^2 \sqrt{\lambda_H \lambda_S} \Rightarrow \lambda_{HS} < \frac{m_S^2}{v^2} + \sqrt{\lambda_H \lambda_S}. \quad (36)$$

Secondly, the validity of the one-loop approximation can be violated by large coupling constants. Thus, we impose the perturbativity of the couplings in high energy scales, while the renormalization group equations (RGE) can be solved at one loop for the couplings λ_{HS} , λ_H , and λ_S (see Appendix B). The RGE evolution of the gauge couplings and the top quark Yukawa coupling remains the same as in the case of the SM. Moreover, the contribution of the higher order operator to the RGEs is omitted since the effective field theory is a weakly coupled theory with $\lambda/M^2 < 10^{-4} \text{ GeV}^{-2}$. Following Ref. [65], the RGE evolution shows that the model remains perturbative up to scales 10–100 TeV depending on the Higgs-singlet coupling, as well as $\lambda_S^{\min} < 8$, is imposed for a reliable perturbative analysis, which is equivalent to $\lambda_{HS} < 5$ with the singlet mass ranging from 0–550 GeV.

Moving on, the tree-level potential has an inherent \mathbb{Z}_2 symmetry, allowing the singlet scalar to act as a dark matter candidate [49,55,59,64,68,69,102–104]. Hence, the unbroken \mathbb{Z}_2 symmetry at zero temperature ensures the stability of the dark matter particle and prohibits the mixing between the Higgs field and the singlet scalar field. As a consequence, the couplings of the Higgs boson to fermions and gauge bosons remain identical to the SM, as well as further constraints from electroweak precision tests, and Higgs

⁵The effective field theory is considered active at the scale $M = 15 \text{ TeV}$ in the following sections.

⁶See Sec. VI.

⁷It is commonly set to $a = 0.1$ for $m_S \geq m_H/2$ [40,65,66,70,101].

coupling modifications are ruled out due to the forbidden Higgs-singlet mixing.

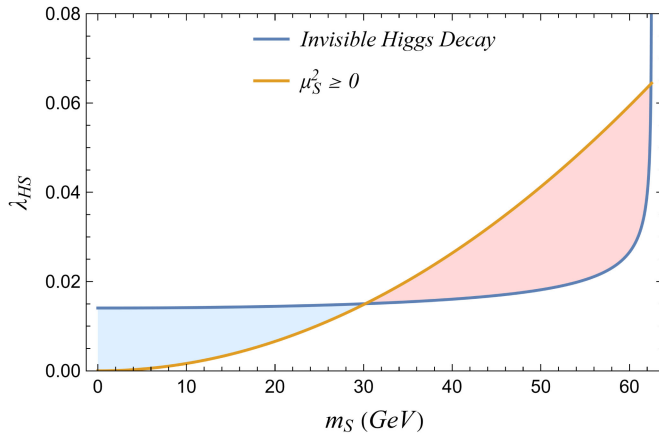
Lastly, the EWBG can be probed by gravitational wave and collider measurements [25,43,44,64,65]. In the case of $m_S > m_H/2$, the number of potential collider signatures is highly restricted due to the forbidden Higgs-singlet mixing. However, future colliders, such as a 100 TeV hadron collider, could test this scenario, probing the direct production of the singlet states, and the modification in the triple Higgs couplings and Zh cross section [65]. Regarding the gravitational waves, their signals from an electroweak first-order phase transition can be detected in the future observatories [43,44,64], such as LISA.

V. CONSTRAINTS FROM INVISIBLE HIGGS DECAY

If $m_S < m_H/2$, the decay $h \rightarrow \phi\phi$ is kinematically allowed, and it contributes to the invisible decay width of the Higgs boson. The ATLAS and CMS experiments have reported numerous results of searches for invisible Higgs decays over the last years. The branching ratio of the Higgs to the invisible singlet sector is set to $BR_{\text{inv}} < 0.11\text{--}0.19$ at 95% CL, where the upper and lower limits of the range correspond to the results from the ATLAS [105] and the CMS Collaboration [106], respectively. In Ref. [107], those results are analyzed further. However, the most recent result from a combination of searches, which is not included in Ref. [107], indicates $BR_{\text{inv}} < 0.107$ at 95% CL [108].

The Higgs decay width to visible channels is $\Gamma_{\text{vis}} = 4.07$ MeV for $m_H = 125$ GeV. Thus, if the branching ratio of the Higgs to the invisible particles is fixed at $BR_{\text{inv}} < 0.19$, the upper bound on the invisible decay width of the Higgs boson is

$$\Gamma(h \rightarrow \phi\phi) < 0.955 \text{ MeV}, \quad (37)$$



where this decay width is given by

$$\Gamma(h \rightarrow \phi\phi) = \frac{\lambda_{\text{HS}}^2 v^2}{32\pi m_H} \sqrt{1 - \frac{4m_S^2}{m_H^2}}. \quad (38)$$

Hence, this bound leads to an additional constraint for the interaction coupling,

$$\lambda_{\text{HS}} < \sqrt{\frac{32\pi m_H}{v^2} \left(1 - \frac{4m_S^2}{m_H^2}\right)^{-1/2} \Gamma_m(h \rightarrow \phi\phi)}, \quad (39)$$

where $\Gamma_m(h \rightarrow \phi\phi)$ is the upper bound on the invisible decay width of the Higgs boson. Requiring $\mu_S^2 \geq 0$ and imposing the previous constraint result in

$$\frac{m_S^2}{v^2} < \lambda_{\text{HS}} < \sqrt{\frac{32\pi m_H}{v^2} \left(1 - \frac{4m_S^2}{m_H^2}\right)^{-1/2} \Gamma_m(h \rightarrow \phi\phi)}, \quad (40)$$

which is completely independent of the coupling λ_S (or equivalently a) and the Wilson coefficient λ .

Consequently, the allowed singlet masses are divided into two regions,

$$m_S \leq 30.19 \text{ GeV} \quad \text{and} \quad m_S \geq 62.43 \text{ GeV},$$

where the two separated regions are merged only for $BR_{\text{inv}} > 0.59$, which does not agree with the experimental data [107]. We gathered the allowed singlet masses in Fig. 2. The lower mass region generally has the upper bound of $\lambda_{\text{HS}} = 0.014$, whereas the higher mass region is characterized by a wider range of values for λ_{HS} , but it has almost a fixed singlet mass.

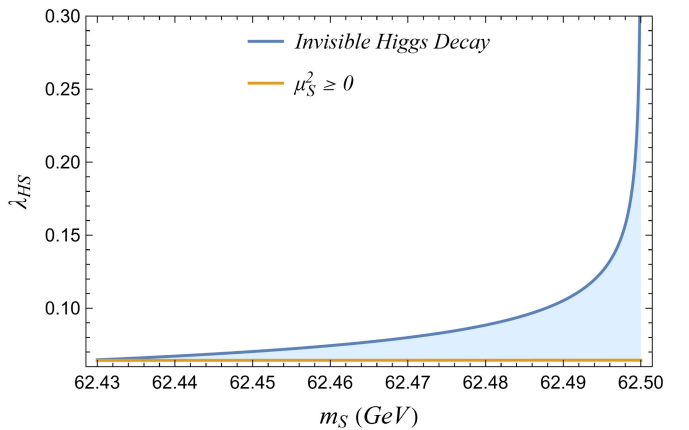


FIG. 2. Left: the parameter space (blue shaded) for $m_S < 62.5$ GeV, which satisfies the invisible Higgs Decay constraint (42) and $\mu_S^2 \geq 0$ setting $BR_{\text{inv}} < 0.19$. Right: the higher mass region, $m_S \geq 62.43$ GeV, which satisfies the invisible Higgs Decay constraint (42) and $\mu_S^2 \geq 0$ setting $BR_{\text{inv}} < 0.19$.

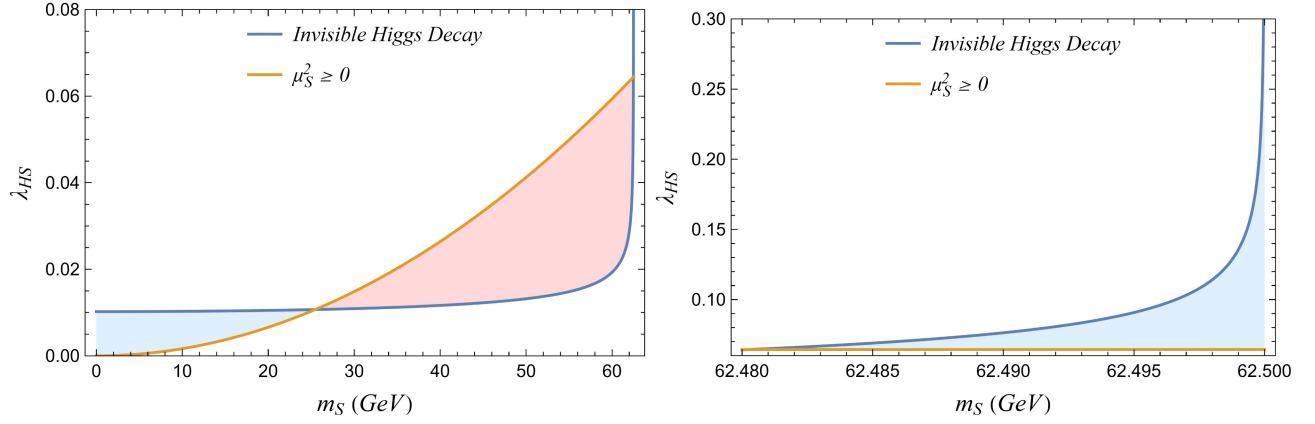


FIG. 3. Left: the parameter space (blue shaded) for $m_S < 62.5$ GeV, which satisfies the invisible Higgs Decay constraint (42) and $\mu_S^2 \geq 0$ setting $BR_{\text{inv}} < 0.11$. Right: the higher mass region, $m_S \geq 62.48$ GeV, which satisfies the invisible Higgs Decay constraint (42) and $\mu_S^2 \geq 0$ setting $BR_{\text{inv}} < 0.11$.

The invisible Higgs boson branching ratio can be also set to the $BR_{\text{inv}} < 0.11$ at 95% CL in order to yield the invisible decay width,

$$\Gamma(h \rightarrow \phi\phi) < 0.503 \text{ MeV}, \quad (41)$$

with the following allowed mass regions that satisfy the condition (40),

$$m_S \leq 25.45 \text{ GeV} \quad \text{and} \quad m_S \geq 62.48 \text{ GeV}.$$

It is immediately obvious that this upper bound further excludes the low-mass region because of the lower maximum value of the coupling λ_{HS} compared to the previous case.

Taking into account the sphaleron rate criterion (30), the parameter space is eliminated further since very low values of the coupling λ_{HS} generate a one-step or a two-step EWPT with a weak first-order phase transition. Therefore, the lower bound on the Higgs-singlet coupling can be higher than the one depicted in Figs. 2 or 3.

VI. THE ELECTROWEAK PHASE TRANSITION IN THE SINGLET-EXTENDED SM: A DETAILED DESCRIPTION

Now we shall analyze the behavior of the singlet-extended effective potential (29) in the full two-dimensional configuration space spanned by the Higgs and the singlet scalar fields (h, ϕ) . We shall describe in some detail the behavior of the full effective potential at finite temperature, and in the next subsections, we shall constrain the free parameters of the model in order to be phenomenologically viable from various aspects. The results presented in Figs. 4 and 5 summarize some of the main results of this paper.

In this work, the electroweak phase transition is considered as a two-step phase transition that consists of a

primary first-order or second-order phase transition in the ϕ direction from the origin $(h, \phi) = (0, 0)$ to a nonzero VEV and a subsequent first-order phase transition from $(0, v'_s)$ to the Higgs vacuum $(v_c, 0)$. In the early Universe, as the temperature decreases, the Higgs minimum is formed, and a barrier is created between the Higgs and the singlet minimum as shown in Figs. 4 and 5. Then a strong first-order phase transition signals the tunneling to the electroweak vacuum, which remains the global minimum at zero temperature. Instead of this cosmological history, the electroweak symmetry breaking could alternatively take place as a one-step strong first-order phase transition from the origin $(0, 0)$ to the electroweak vacuum $(v_c, 0)$ along the Higgs direction, while the singlet vacuum is stabilized on the origin with zero VEV. This one-step scenario can be driven by loop effects requiring $\mu_S^2 < 0$ [38,65,69]. A comprehensive study on the classification of numerous models to thermally driven, tree-level driven, and loop-driven is given in Ref. [38]. Nevertheless, a one-step phase transition can be also realized in the case of $\mu_S^2 > 0$ due to thermal effects.

Furthermore, an instability can be developed along the singlet's direction at extremely high temperatures for large values of the couplings λ , λ_{HS} , and λ_S . This instability can also take place without the dimension-six operator, which was included in the Lagrangian, but in our model, it is mainly caused by large λ and a , which importantly affect the singlet's effective potential. However, this behavior does not alter the above discussion because the strong first-order transition is still realized with $T_c \ll T_s$. Nevertheless we need to stress that such an instability could lead to a high temperature transition from the $\langle s \rangle = 0$ minimum to the $\langle s \rangle = v_s$ vacuum, at a temperature way higher than the one corresponding to the electroweak phase transition. This phase transition would generate defects such as domain walls, and these could remain as remnants of this phase transition. This feature is mentionable, and it occurs for the

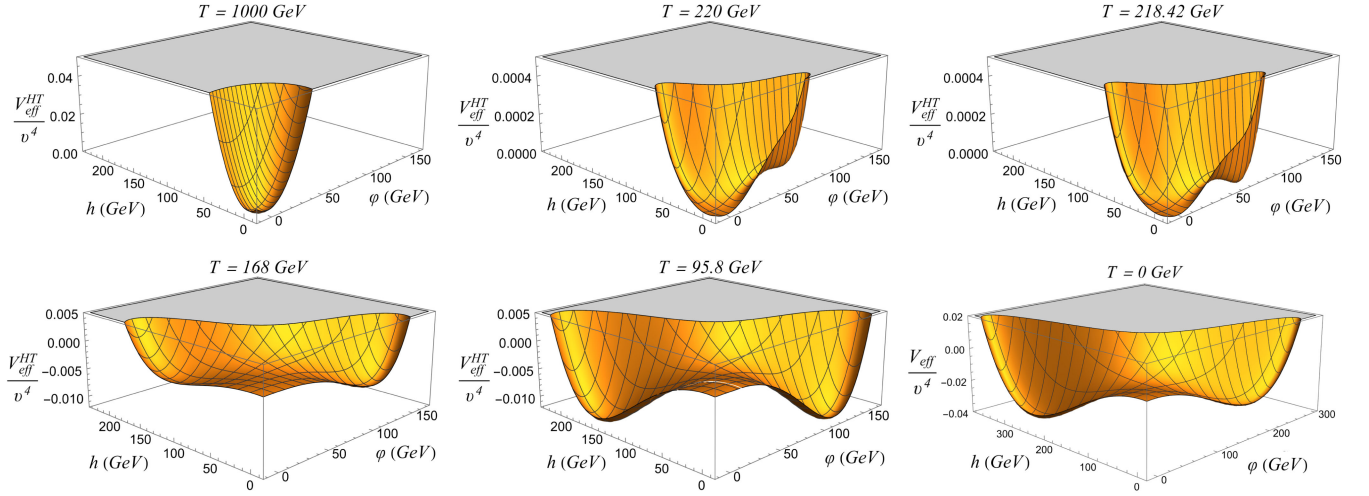


FIG. 4. The full effective potential during the strong electroweak phase transition as the temperature decreases. In this example, the singlet's phase transition is first order using a point of the parameter space with $m_S = 500$ GeV, $\lambda_{HS} = 4.3$, $\lambda/M^2 \simeq 2 \times 10^{-5}$ GeV $^{-2}$, and $a = 0.1$.

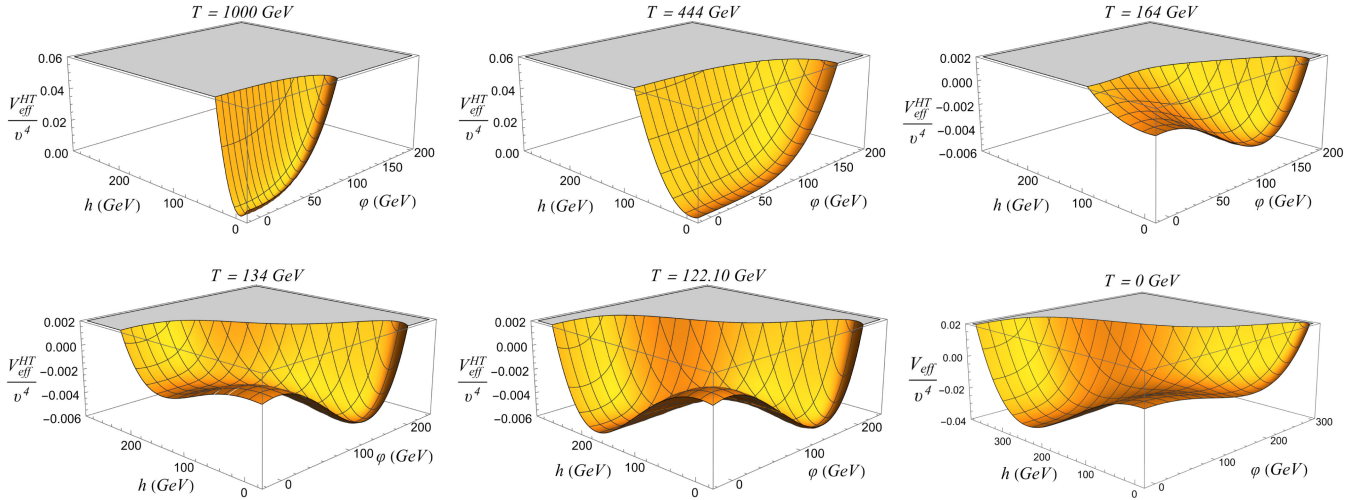


FIG. 5. The full effective potential during the strong electroweak phase transition as the temperature decreases. In this example, the singlet's phase transition is second order using a point of the parameter space with $m_S = 62.5$ GeV, $\lambda_{HS} = 0.15$, $\lambda/M^2 \simeq 2 \times 10^{-5}$ GeV $^{-2}$, and $a = 0.1$.

aforementioned values of the parameter; however, it relies on the fact that the temperature indeed reached such high values, which is not certain. We needed to report this because it is a peculiar and mentionable feature, which must be treated with reluctance, however, due to the extreme temperature that it occurs and also because if it occurs, it occurs well before the electroweak phase transition. More importantly, from a physical point of view, perturbation theory does not break in the singlet sector. However, the ratio of the singlet mass over the corresponding temperature would be nearly zero, $m_S/T_s \sim 0$; thus, normally, such high temperatures and the corresponding transitions in the effective potential should be disregarded, in the same way we disregarded the effect of small mass

quarks in the Higgs effective potential. We mention this issue for completeness though and in order to provide a spherical and complete view of the parameter space for the convenience of the reader.

In addition, a common issue in this thermal history arises when topological defects emerge due to the spontaneous symmetry breaking of the discrete \mathbb{Z}_2 symmetry, while the singlet scalar field acquires a nonzero VEV at a high temperature [109]. Namely, electroweak baryogenesis can be highly affected by the generated domain walls after the high-temperature spontaneous symmetry breaking. Recently, it was shown in Ref. [110] that the inclusion of a dimension-six singlet scalar field operator in the usual real singlet extensions can resolve this problem considering

a scenario in which the vacuum state never respected the \mathbb{Z}_2 symmetry. This scenario is not examined further in this study, leaving such an analysis and the implications of topological defects for future work. However, it is noticeable that in our model, the \mathbb{Z}_2 symmetry could be never restored at high temperature due to the aforementioned instability developed along the ϕ direction in the effective potential. Namely, one observes that the singlet VEV remains nonzero for large λ and a at extremely high temperatures $T > T_c$. As a result, in these cases, the \mathbb{Z}_2 symmetry is not restored, and the issue of the domain walls is avoided.

Finally, the influence of the higher order operator on the electroweak phase transition can be comprehensively understood by its mathematical aspects. In the Higgs direction, the nonzero Wilson coefficient changes the thermal mass of the singlet (21), where λ is compared with the couplings λ_{HS} and λ_S , which is then expressed in terms of singlet mass m_S , the coupling λ_{HS} , and the parameter a . This means that the relation between their values can play an essential role for the effect of the higher order operator. In the ϕ direction, on the other hand, the Wilson coefficient mainly contributes to the effective mass of the Higgs boson (4), the Goldstone bosons (5), and the singlet (6), while the thermal mass of the singlet remains the same as in the Higgs direction. As a consequence, in the direction with $h = 0$, the effect of the Wilson coefficient is primarily determined by the coupling λ_{HS} and the singlet mass m_S . Therefore, it is worth mentioning that the nonzero Wilson coefficient significantly changes the effective potential (29) in the ϕ direction.

In the next subsections, the two-step strong electroweak phase transition is studied by dividing the parameter space of the singlet extension with the dimension-six operator in three regions: the low-mass region ($m_S < m_H/2$), the Higgs resonance region ($m_S = m_H/2$), and the high-mass region ($m_S > m_H/2$).

A. High-mass region: $m_S > m_H/2$

First of all, the two-step electroweak phase transition can be described by the parameter space for $m_H < 2m_S$ in Fig. 6 with zero Wilson coefficient, adopting the common parametrization with $a = 0.1$. As it has been previously mentioned, this parameter space includes a number of small regions with a one-step electroweak phase transition. In particular, it was found that the parameter space with $\mu_S \lesssim 90$ GeV corresponds to a region with both scenarios. On the other hand, imposing the criterion for a strong first-order phase transition reduces the generic two-step parameter space with $\lambda = 0$. More specifically, it is mainly changed for $m_S > 200$ GeV and low Higgs-singlet couplings as the criterion (30) requires higher coupling⁸ λ_{HS} in

⁸The difference between the lowest λ_{HS} for satisfying the sphaleron rate criterion with lower bound 0.6 and 1 is negligible.

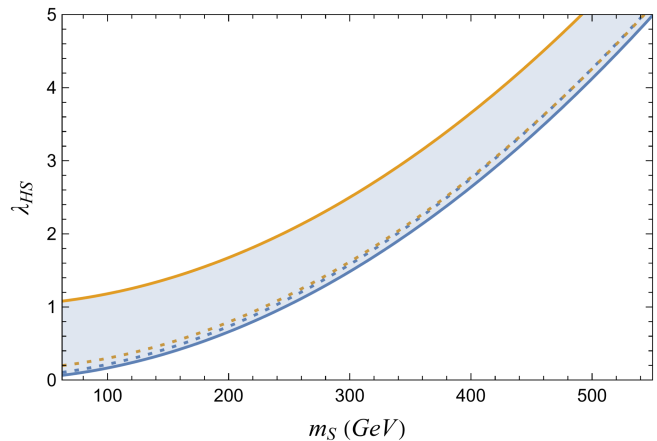


FIG. 6. The blue region is the parameter space of the singlet model for a two-step electroweak phase transition with $m_S > m_H/2$, $a = 0.1$, and $\lambda = 0$. The orange dotted line describes the constant $\mu_S = 90$ GeV. The parameter space of the strong two-step electroweak phase transition with $v_c/T_c > 1$ corresponds to the blue region, which is bounded from below by the blue dotted line. The critical temperature in this parameter space varies from $T_c \simeq 30$ –140 GeV.

comparison with the generic case of a two-step phase transition. Those higher values of the lower bound for the coupling λ_{HS} vary with different singlet masses, and they are depicted by the blue dotted line in Fig. 6. These results generally agree with similar studies [64,65,70,101]. The renormalization scale dependence and other theoretical uncertainties in the perturbative analysis (which are discussed in Refs. [66,72–74]) may introduce small differences between our results and the literature. Moreover, the authors of Ref. [70] claimed that larger parts of the two-step electroweak phase transition parameter space are ruled out since relativistic speeds during the phase transition must not be reached by the expanding bubble walls, and it is required that bubbles do nucleate at finite temperature. Nonetheless, we do not consider these effects in the present study, leaving such improvement for future work.

The presence of the higher order operator with $\lambda < 10^2$ does not noticeably affect the aforementioned parameter space of the strong electroweak phase transition. The lowest coupling λ_{HS} for a strong phase transition slightly increases with $\lambda \lesssim 10^3$, and the critical temperature is significantly increased, whereas the ratio v_c/T_c shows a downward trend. This effect is strengthened by very high and very low singlet masses. On the other hand, the maximum value of the coupling λ_{HS} , which is shown in Fig. 6, is not changed by the higher order operator. In this case, the effect of the nonzero Wilson coefficient is highly weakened by lower singlet masses. The comparison between the parameter space of the singlet extension with $\lambda = 0$ and $\lambda = 10^4$ is presented in Fig. 7. It is clearly seen that the influence of the dimension-six operator is not

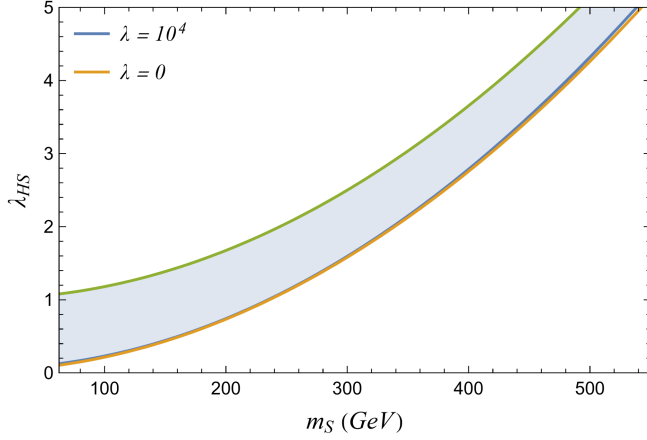


FIG. 7. The parameter space (blue region) of the singlet extension with a dimension-six operator ($\lambda = 10^4$) in order to realize a strong two-step electroweak phase transition ($v_c/T_c > 1$). The orange line shows the lower bound of the parameter space of the singlet extension, which is represented by a blue dotted line in Fig. 6. In both cases, we take $a = 0.1$.

crucial for $a = 0.1$. On the contrary, this behavior dramatically alters for higher values of the parameter a , and it is extensively studied for lower singlet masses.

The behavior of the full effective potential at finite temperature is depicted in Fig. 4 for the case at hand by taking into account all the phenomenological constraints obtained in this subsection and for various temperatures. In this example, the singlet's phase transition is first order using a point of the parameter space with $m_S = 500$ GeV, $\lambda_{\text{HS}} = 4.3$, $\lambda/M^2 \simeq 2 \times 10^{-5}$ GeV $^{-2}$, and $a = 0.1$, but it can also be a second-order phase transition for lower singlet masses and Higgs-singlet couplings. As it can be seen, at high temperatures, the effective potential is symmetric, and as the temperature decreases, the singlet vacuum with a barrier between the second vacuum and the origin is developed. As the temperature decreases, the Higgs vacuum is generated with another barrier between the latter and the origin also existing. Accordingly, the Higgs vacuum is deeper than the singlet vacuum, and the electroweak symmetry breaking phase transition occurs.

B. Higgs resonance region: $m_S = m_H/2$

The Higgs resonance region is highly motivated by dark matter physics since the singlet should have a mass near $m_S = 62.5$ GeV as a viable dark matter candidate [102–104], and it is strongly restricted by the direct dark matter searches by LUX, XENON1T, and XENONnT experiments [49,59,64,102–104]. While in the majority of the parameter space without the dimension-six operator, the assumption of the real singlet as a dark matter candidate is inconsistent with a strong first-order electroweak phase transition, it has been shown that in the Higgs resonance region, the dark matter relic density can constitute an

important proportion of the total observed dark matter density [102–104].

Additionally, the full effective potential at finite temperature is illustrated in Fig. 5 using a point of the parameter space with $\lambda_{\text{HS}} = 0.15$, $\lambda/M^2 \simeq 2 \times 10^{-5}$ GeV $^{-2}$, and $a = 0.1$, and a similar behavior is followed in the total parameter space with $m_S = m_H/2$. The singlet's phase transition is generally second order in this region in which the two-step electroweak phase transition satisfies the sphaleron rate criterion.

Firstly, the common value of $a = 0.1$ is selected in order to compute the critical temperature T_c , the critical temperature T_s of the singlet's phase transition and the sphaleron rate criterion for various values of the Wilson coefficient, and the Higgs-singlet coupling, which are presented in Figs. 8–11. The electroweak phase transition is considerably affected by the higher order operator for $\lambda > 10^3$, and the parameter space is restricted, as the ratio v_c/T_c drops for a nonzero Wilson coefficient, and a higher λ_{HS} is necessary to generate the strong electroweak phase transition. Moreover, the phase transition in the ϕ direction occurs at a very high temperature for $\lambda/M^2 \simeq 4 \times 10^{-5}$ GeV $^{-2}$, which shows the strong influence of the higher order operator on the singlet's dynamics.

On the other hand, the parameter space of the strong electroweak phase transition is expanded by taking $a > 0.4$. This is an important feature of our model that we need to further highlight at this point. This is clearly illustrated in the case of $a = 1$ in Fig. 10, where the criterion $v_c/T_c > 1$ can be satisfied by much lower λ_{HS} compared to the model with zero Wilson coefficient. As a result, if $\lambda/M^2 \gtrsim 10^{-4}$ GeV $^{-2}$, a strong electroweak phase transition can be realized for every low Higgs-singlet coupling with $\mu_S^2 > 0$. Hence, the higher order operator could assist a strong electroweak phase transition in regions of the parameter space that were excluded in the previous singlet extensions of the SM.

Regarding the singlet's phase transition, the trend of the critical temperature T_s is similar to the case of $a < 0.4$, and T_s sharply increases as the Wilson coefficient increases. In addition, the previously mentioned instability in the ϕ direction takes place for $\lambda > 3650$ and $\lambda_{\text{HS}} > 0.52$ with $a = 1$, which is also showcased by the fact that $\lambda_{\text{HS}} = 0.52$ leads to $T_s \simeq 8768$ GeV. It is noticeable that lower values of a lead to this instability for higher values of the Wilson coefficient and the Higgs-singlet coupling.

In Figs. 8 and 10, the critical temperature with $\lambda \neq 0$ approaches the critical temperature with $\lambda = 0$ for larger values of the Higgs-singlet coupling. This behavior shows that the effect of the higher order operator is stronger for low values of λ_{HS} . This is also apparent for the ratio for the sphaleron rate criterion in Figs. 9 and 10. However, in the case of $a = 0.1$, the influence of the higher order operator is maximized for an intermediate low value of the Higgs-singlet coupling and not for the lower values.

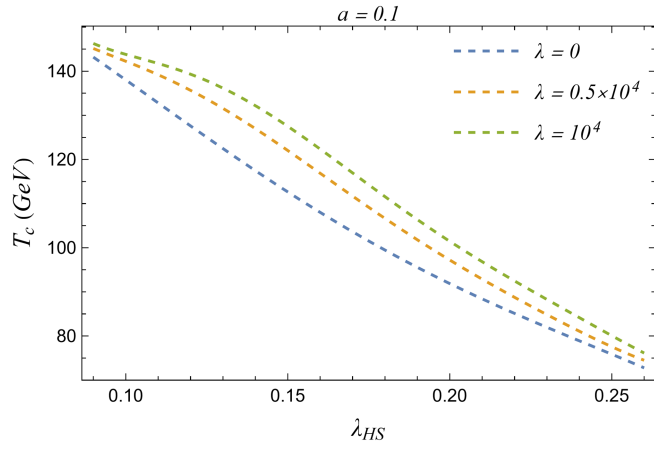


FIG. 8. The critical temperature (T_c) as a function of the Higgs-singlet coupling (λ_{HS}) for $m_S = 62.5$ GeV and $a = 0.1$.

Finally, it is essential to mention that if the value of $a < 0.1$, at zero temperature, the Higgs VEV v is not much deeper than the singlet VEV v_s . Namely, the condition (32) is satisfied for every a in Eq. (35), but low values of a do not satisfy the condition,

$$V_0(0, v_s) \gg V_0(v, 0), \quad (42)$$

which ensures that the Higgs vacuum is by far more energetically favorable compared to the singlet vacuum.

C. Low-mass region: $m_S < m_H/2$

In the low-mass region, the behavior of the full effective potential remains the same as in the Higgs resonance region, while the high-temperature phase transition in the ϕ direction is primarily second-order in the allowed parameter space.

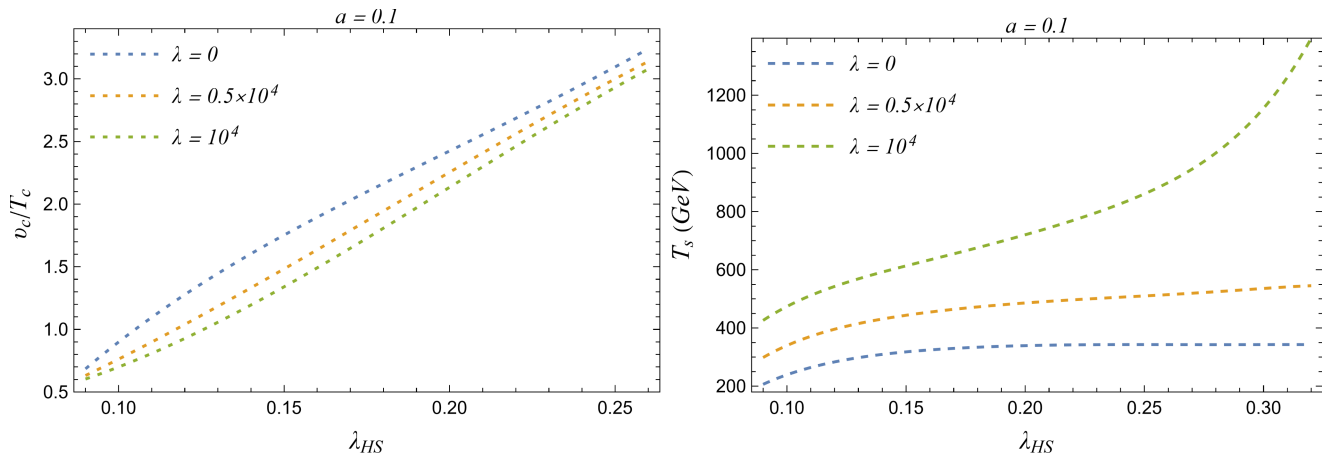


FIG. 9. Left: the sphaleron rate criterion as a function of the coupling λ_{HS} for $m_S = 62.5$ GeV and $a = 0.1$ in the case of zero and nonzero Wilson coefficient. Right: the critical temperature of the singlet's second-order phase transition T_s as a function of the coupling λ_{HS} for $m_S = 62.5$ GeV and $a = 0.1$.

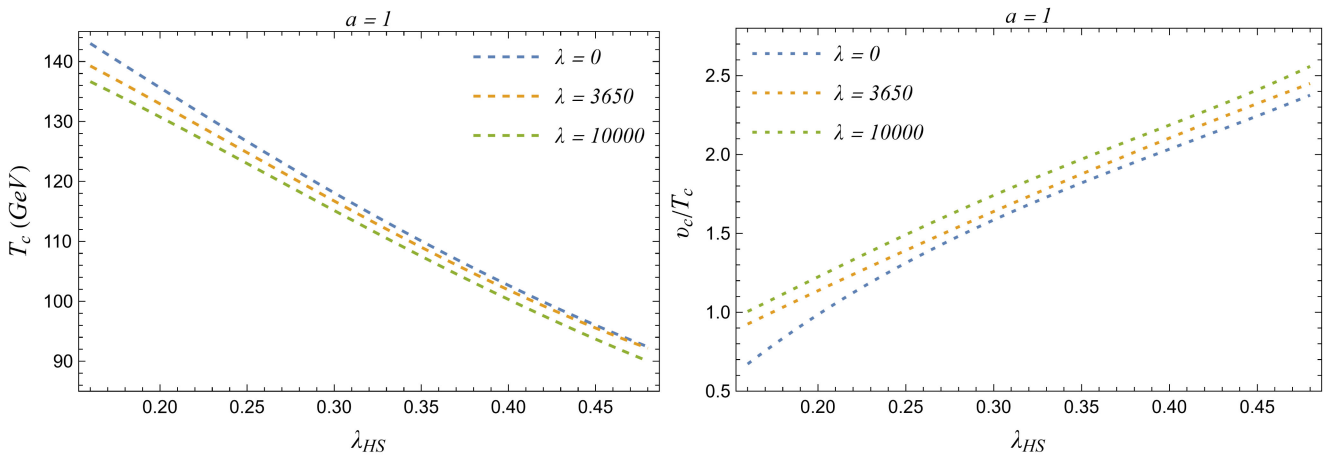


FIG. 10. The electroweak phase transition with $m_S = 62.5$ GeV and $a = 1$: Left: the critical temperature (T_c) as a function of the Higgs-singlet coupling (λ_{HS}). Right: the sphaleron rate criterion as a function of the coupling λ_{HS} in the case of zero and nonzero Wilson coefficient.

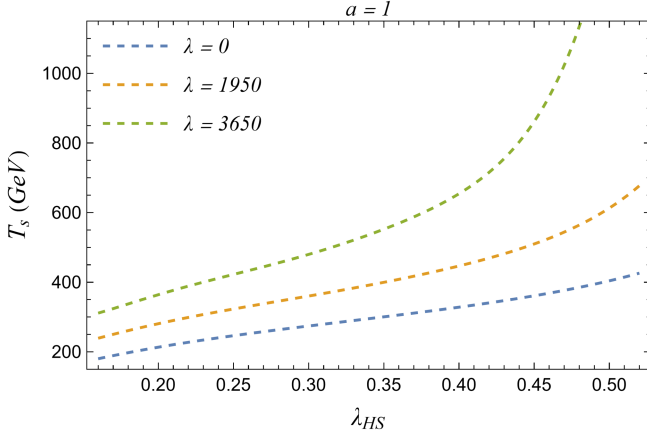


FIG. 11. The critical temperature of the singlet's second-order phase transition T_s as a function of the coupling λ_{HS} for $m_S = 62.5$ GeV and $a = 1$ in the case of zero and nonzero Wilson coefficient.

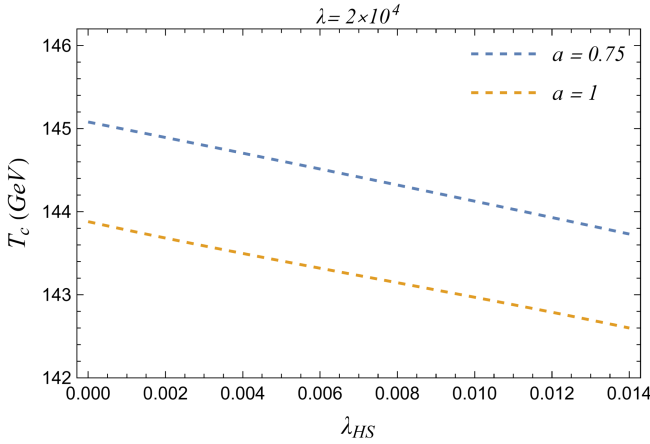


FIG. 12. The critical temperature as a function of the Higgs-singlet coupling for $a = 0.75$ and 1 and $m_S \leq 0.1$ GeV.

It has been already shown that the parameter space for $m_S < m_H/2$ is severely eliminated by the invisible decay width of the Higgs boson and the condition $\mu_S^2 > 0$. It is initially assumed that the branching ratio of the Higgs boson to invisible particles is set to $BR_{\text{inv}} < 0.19$. However, the lower mass region $m_S \lesssim 30$ GeV, which is allowed by these constraints, is completely excluded by the sphaleron rate criterion considering $\lambda = 0$ and $a \gtrsim 0.05$ due to the low values of the Higgs-singlet coupling. On the contrary, large values of $\lambda > 10^3$ and $a \gtrsim 0.05$ can easily assist the strong phase transition for $m_S \leq 1$ GeV. This is clearly illustrated if we take $\lambda = 2 \times 10^4$, and $a = 0.75$ as a strong electroweak phase transition ($v_c/T_c > 0.6$) occurs for every coupling λ_{HS} and $m_S < 10$ GeV. This is shown in Fig. 12. More specifically, the lower bound of λ_{HS} with a singlet mass $m_S = 0.1$ GeV and $\lambda = 2 \times 10^4$ can generate a strong electroweak phase transition, and it is at least 10^6 times smaller than the corresponding value in the singlet extension without the higher order operator.

Therefore, the presence of the higher order operator allows very low interaction couplings, which easily avoid the constraint imposed by the branching ratio $BR_{\text{inv}} < 0.10$.

In contrast, the previous behavior is dramatically changed for values $a \lesssim 0.05$, as the zero Wilson coefficient can lead to a strong first-order phase transition, whereas the presence of the higher order operator weakens the electroweak phase transition. The electroweak phase transition with zero Wilson coefficient mainly occurs for $m_S < 10$ GeV in order to have a two-step phase transition, but this upper limit on the mass increases for very low values of the parameter a and λ_{HS} . This behavior is also illustrated in Fig. 13 since it shows that the lowest allowed value of λ_{HS} decreases as the parameter a drops for a given singlet mass.

Some typical results are presented for $m_S \leq 1$ GeV and $a = 0.001$ in Figs. 14 and 15. Firstly, it can be clearly seen

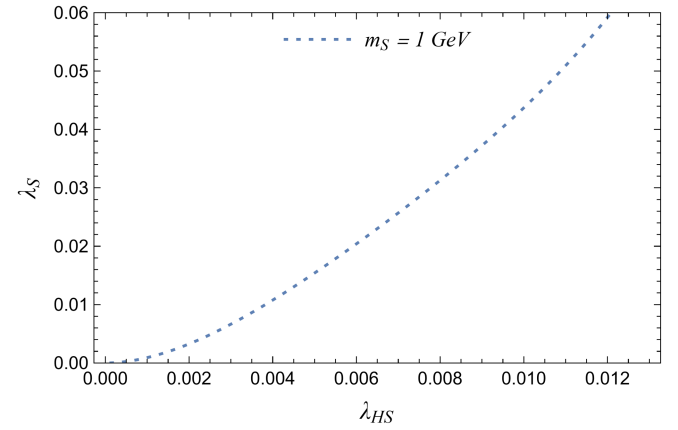


FIG. 13. The dependence of the lowest λ_{HS} , which is allowed by all the previous constraints imposing the criterion $v_c/T_c > 0.6$, on the parameter a for $m_S = 1$ GeV and $\lambda = 0$. This dependence was numerically computed to explain qualitatively that the parameter space expands its lower bound for low values of the quartic coupling λ_S .

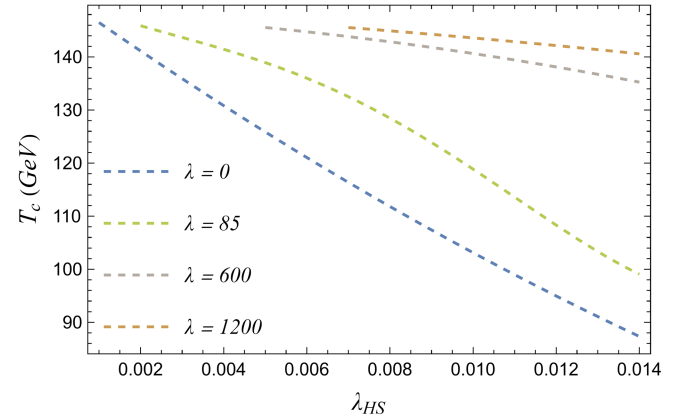


FIG. 14. The critical temperature as a function of the coupling λ_{HS} for $m_S \leq 1$ GeV and $a = 0.001$ in the case of zero and nonzero Wilson coefficient $\lambda = 0$ (blue), 85 (green), 600 (gray), 1200 (brown).

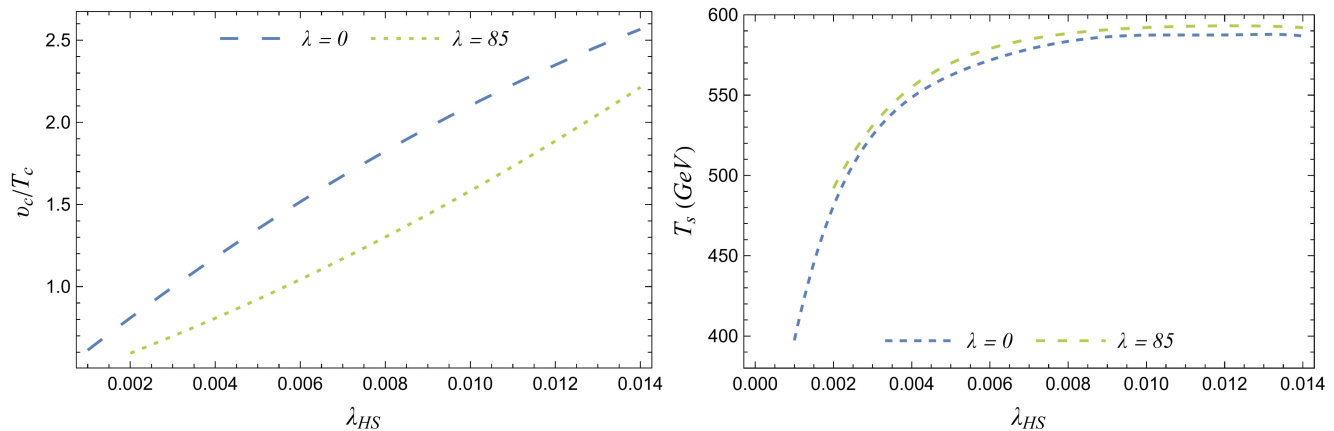


FIG. 15. Left: the sphaleron rate criterion as a function of the coupling λ_{HS} for $m_S \leq 1$ GeV and $a = 0.001$ in the case of zero and nonzero Wilson coefficient. Right: the critical temperature of the singlet's second-order phase transition T_s as a function of the coupling λ_{HS} for $m_S \leq 0.1$ GeV and $a = 0.001$ in the case of zero and nonzero Wilson coefficient.

that the lower bound of λ_{HS} is strongly constrained by a nonzero total Wilson coefficient $\lambda/M^2 \simeq 10^{-7} - 10^{-5}$ GeV $^{-2}$. In addition, the full effective potential around the critical temperature T_c remains the same for masses between 0–1 GeV with maximum deviations in the critical temperature of the order of 10^{-2} . In Fig. 14, the trend of critical temperature T_c is similar to one in the previous mass region, whereas the temperature T_s in Fig. 15 stabilizes for large values of λ_{HS} , in contrast to the behavior described in the previous sections.

In the case of $BR_{\text{inv}} < 0.11$ in the lower mass region, the previous conclusions do not change as this constraint only decreases the maximum allowed value of the Higgs-singlet coupling to $\lambda_{HS}^{\text{max}} = 0.10$, which subsequently excludes some scenarios, especially for $\lambda = 0$.

In the second region of the parameter space for $m_S < m_H/2$, the singlet mass is strictly restricted to almost the half mass of the Higgs boson due to constraints in Eq. (40) (Figs. 2 and 3). As a result, there is no noticeable difference between this case and the Higgs resonance regarding the second step in the two-step electroweak phase transition, while the phase transition in the ϕ direction is slightly affected. Namely, the results on the critical temperature T_c and the Higgs VEV v_c remain the same as the results in the previous section.

Assuming $BR_{\text{inv}} < 0.19$, the constraint (40) leads to singlet mass $m_S = 62.48$ GeV and coupling $\lambda_{HS} = 0.88$ as the only strong electroweak phase transition scenario⁹ for $a = 0.1$ in the standard singlet extension. Thus, the constraint (40) imposes that $m_S \geq 62.48$ GeV and leads to a narrow parameter space.¹⁰ On the other hand, the higher

order operator can decrease the lower bound on the Higgs-singlet coupling due to the sphaleron rate criterion as it was discussed in the previous section. It is remarkable that in the higher mass region, the coupling $\lambda_{HS} > 0.065$ [allowed by Eq. (40)] generates a viable electroweak phase transition for $\lambda/M^2 \simeq 9 \times 10^{-5}$ GeV $^{-2}$ and $a = 0.75$. Consequently, the inclusion of the dimension-six operator can contribute to the occurrence of a strong electroweak first-order phase transition in the higher mass region of the parameter space for $m_S < m_H/2$. This discussion is analogous in the case of $BR_{\text{inv}} < 0.11$ because the lower bound of the Higgs-singlet coupling remains unaffected, whereas the size of the parameter space differs, with the parameter space being highly restricted for $m_S < 62.499$ GeV.

VII. CONCLUSIONS AND DISCUSSION

Our current perception for the Universe during its primordial classical and quantum evolution stages is rather vague. Too many questions have to be answered, and the current and future CMB and gravitational wave experiments are expected to shed light on these stages of our Universe's evolution. The mechanism that gave masses to the matter particles is the electroweak symmetry breaking, and this is believed to have occurred via a first-order phase transition. However, the electroweak phase transition in the SM is not a sufficiently strong first-order phase transition. To this end, in this article, we studied the electroweak phase transition in the context of the real singlet extensions of the SM, including dimension-six non-renormalizable operators, which couple the singlet scalar field with the Higgs doublet. We showed that the electroweak phase transition occurs as a two-step phase transition, which consists of the singlet's phase transition at high temperature and a subsequent strong first-order phase transition in the Higgs and SM

⁹The sphaleron rate criterion is satisfied: $\frac{v_c}{T_c} \simeq 0.61$.

¹⁰The maximum value of λ_{HS} in Eq. (39) sharply increases as it approaches half of the Higgs mass. This maximum value for $m_S = 62.49998$ GeV reaches nearly half of the upper bound of λ_{HS} in the parameter space shown in Fig. 7.

sector. In addition, considering a viable CP -violation source, such as a dimension-six operator, which couples the singlet to the top quark mass, the electroweak baryogenesis can be realized to describe the baryon asymmetry in the current Universe. This scenario is also compatible with assuming the singlet particle as dark matter candidate with mass nearly half of the Higgs mass, which is highly restricted by the direct dark matter searches. As we previously discussed, the parameter space is majorly reduced by the sphaleron rate criterion, the vacuum structure, the perturbativity of couplings, and the invisible Higgs decay width. Consequently, we studied the two-step strong electroweak phase transition, which respects those constraints for $m_S = 0\text{--}550$ GeV. In this model, the critical temperature of the first-order phase transition varies from $T_c \simeq 30\text{--}200$ GeV depending on the parameters of the model.

The impact of the dimension-six operator is summarized as follows:

- (i) The presence of the dimension-six operator mainly modifies the thermal mass of the singlet in the Higgs direction, which alters the first-order phase transition, while the singlet's phase transition is strongly affected by the nonzero Wilson coefficient, and its critical temperature increases for higher Wilson coefficients. In addition, the effect of the higher order operator is washed out by large values of the Higgs-singlet coupling and is weakened for coefficients $\lambda < 10^3$ in most cases.
- (ii) The dimension-six operator can generally assist in generating the strong electroweak phase transition for low Higgs-singlet couplings, which were not allowed in the standard singlet extensions of the SM.
- (iii) The parameter space of our model for $m_S > m_H/2$ and $a = 0.1$ remains approximately the same as in the standard singlet extension. In the Higgs resonance region, the singlet particle could be a dark matter candidate, and the parameter space for $a > 0.4$ is expanded for large values of the Wilson coefficient, whereas this trend is reversed for $a < 0.4$.
- (iv) The low-mass region is significantly excluded by the invisible Higgs decay width and the sphaleron rate criterion in the context of the standard singlet extensions. Nevertheless, a strong electroweak phase transition can be generated for low singlet masses $m_S < m_H/2$ by including the dimension-six operator with $\lambda/M^2 \gtrsim 5 \times 10^{-6} \text{ GeV}^{-2}$ and $a \gtrsim 0.05$.

A study we did not include in our analysis is the study of the stochastic gravitational wave background that corresponds to the first-order phase transitions occurring in our model. It is expected that the collisions between the bubbles of vacua during the first-order phase transition can generate a stochastic gravitational wave background

in the frequencies probed by current and future gravitational wave experiments. We aim to analyze the stochastic gravitational wave background generated by our model in a near future work.

ACKNOWLEDGMENTS

This research has been funded by the Committee of Science of the Ministry of Education and Science of the Republic of Kazakhstan (V. K. O.) (Grant No. AP19674478).

APPENDIX A: ELECTROWEAK PHASE TRANSITION IN THE SM

The electroweak phase transition can be realized in the context of the SM as a first-order phase transition [16,40,81,83,86,91,111,112], but it is insufficiently strong to generate the baryon asymmetry. The dynamics of the phase transition are described by the temperature-dependent effective potential of the Higgs field including the dominant contributions of the gauge bosons, the top quark, and the Goldstone bosons. This effective potential is explicitly presented in Sec. II, and in the Arnold-Espinosa scheme, it is written as

$$\begin{aligned}
 V_{\text{eff}}^{\text{SM}}(h, T) = & -\frac{\mu_H^2}{2} h^2 + \frac{\lambda_H}{4} h^4 \\
 & + \sum_i (-1)^{F_i n_i} \frac{m_i^4(h)}{64\pi^2} \left[\ln \left(\frac{m_i^2(h)}{\mu_R^2} \right) - C_i \right] \\
 & + \sum_i \frac{n_i T^4}{2\pi^2} J_B \left(\frac{m_i^2(h)}{T^2} \right) - 12 \frac{T^4}{2\pi^2} J_F \left(\frac{m_t^2(h)}{T^2} \right) \\
 & + \sum_i \frac{\bar{n}_i T}{12\pi} [m_i^3(h) - (M_i^2(h, T))^{3/2}], \quad (\text{A1})
 \end{aligned}$$

where $i = \{h, \chi, W, Z, \gamma\}$ corresponds to the bosons in the SM.

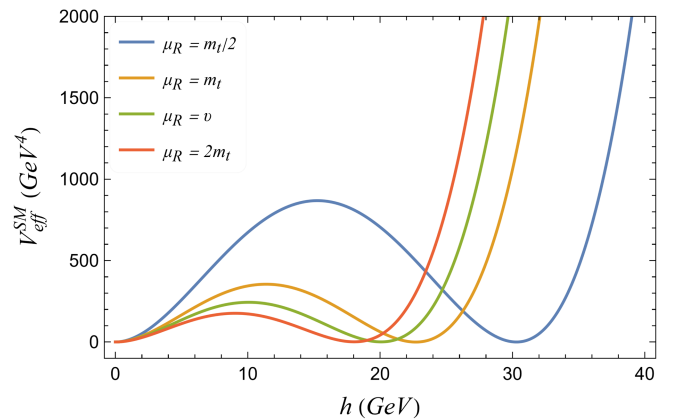


FIG. 16. The full effective potential of the SM at the critical temperature for numerous renormalization scales $\mu_R = m_t/2$ (blue), m_t (orange), v (green), and $2m_t$ (red).

The high-temperature expansion of the thermal functions (15) and (16) for the temperature-dependent one-loop effective potential is valid with very high accuracy in the case of the phase transition. Hence, the high-temperature expansion is implemented in the full effective potential, which reads

$$\begin{aligned}
V_{\text{eff}}^{\text{SM}}(h, T) = & -\frac{\mu_H^2}{2}h^2 + \frac{\lambda_H}{4}h^4 + \frac{m_h^2(h)}{24}T^2 - \frac{T}{12\pi}[m_h^2(h) + \Pi_h(T)]^{3/2} + \frac{m_h^4(h)}{64\pi^2}\left[\ln\left(\frac{a_b T^2}{\mu_R^2}\right) - \frac{3}{2}\right] + \frac{3m_\chi^2(h)}{24}T^2 \\
& - \frac{3T}{12\pi}[m_\chi^2(h) + \Pi_\chi(T)]^{3/2} + \frac{3m_\chi^4(h)}{64\pi^2}\left[\ln\left(\frac{a_b T^2}{\mu_R^2}\right) - \frac{3}{2}\right] + \frac{6m_W^2(h)}{24}T^2 - \frac{4T}{12\pi}m_W^3(h) \\
& - \frac{2T}{12\pi}[m_W^2(h) + \Pi_{W_L}(T)]^{3/2} + \frac{6m_W^4(h)}{64\pi^2}\left[\ln\left(\frac{a_b T^2}{\mu_R^2}\right) - \frac{5}{6}\right] + \frac{3m_Z^2(h)}{24}T^2 - \frac{2T}{12\pi}m_Z^3(h) - \frac{T}{12\pi}[M_{Z_L}^2(h, T)]^{3/2} \\
& + \frac{3m_Z^4(h)}{64\pi^2}\left[\ln\left(\frac{a_b T^2}{\mu_R^2}\right) - \frac{5}{6}\right] + \frac{12m_t^2(h)}{48}T^2 - \frac{12m_t^4(h)}{64\pi^2}\left[\ln\left(\frac{a_f T^2}{\mu_R^2}\right) - \frac{3}{2}\right] - \frac{T}{12\pi}[M_{\gamma_L}^2(h, T)]^{3/2}, \quad (\text{A2})
\end{aligned}$$

where the effective masses are given by

$$m_h^2(h) = -\mu_H^2 + 3\lambda_H h^2, \quad (\text{A3})$$

$$m_\chi^2(h, \phi) = -\mu_H^2 + \lambda_H h^2, \quad (\text{A4})$$

and Eqs. (7)–(9), while the temperature-dependent self-energy of the Higgs and the Goldstone bosons reads

$$\Pi_h(T) = \Pi_\chi(T) = \left(\frac{3g^2}{16} + \frac{g^2}{16} + \frac{y_t^2}{4} + \frac{\lambda_H}{2}\right)T^2, \quad (\text{A5})$$

and the thermal masses of the gauge bosons are given by Eqs. (22), (26), and (27).

The electroweak phase transition is studied by varying the renormalization scale for different values. The full effective potential (A2) is illustrated in Fig. 16 for $\mu_R = m_t/2$ (blue), m_t (orange), v (green), and $2m_t$ (red).

It is immediately apparent that the sphaleron rate criterion is not satisfied as well as the maximum ratio is achieved for $\mu_R = m_t/2$ with $v_c/T_c \simeq 0.2 < 0.6$; namely, the electroweak phase transition is not a strong enough first-order phase transition.¹¹ Similar calculations can be found in Refs. [16,40,81,83,91]. In the context of the perturbative analysis, the sphaleron rate criterion can be translated into an upper bound on the mass of the Higgs boson, such as $m_h \lesssim 42$ GeV [81], which showcases the lack of a strong phase transition in SM, whereas this bound is $m_h \lesssim 72\text{--}80$ GeV in lattice calculations [113–116]. While the height of the barrier in the effective potential and the Higgs VEV during the phase transition clearly change for different renormalization scales, the critical

¹¹Likewise, the authors of Ref. [83] argued that the sphaleron rate criterion is not satisfied for $m_h = 125$ GeV in SM. In particular, they calculated that $v_c/T_c \simeq 0.2$ for $m_h = 120$ GeV and $m_t = 170$ GeV, considering the high-temperature expansion without the daisy resummation.

temperature is slightly dropped by less than 1% for higher values of the renormalization scale as presented in Table I.

APPENDIX B: ONE-LOOP BETA FUNCTIONS

The RGEs for the parameters of the real singlet extension to the SM are presented here:

$$\begin{aligned}
16\pi^2\beta_{\lambda_H} = & 24\lambda_H^2 - 3(3g^2 + g^2 - 4y_t^2)\lambda_H + \frac{1}{2}\lambda_{\text{HS}}^2 \\
& + \frac{3}{8}(3g^4 + 2g^2g^2 + g^2) - 6y_t^4, \quad (\text{B1})
\end{aligned}$$

$$\begin{aligned}
16\pi^2\beta_{\lambda_{\text{HS}}} = & 4\lambda_{\text{HS}}^2 + \left(12\lambda_H + 6\lambda_S + 6y_t^2 - \frac{9}{2}g^2 - \frac{3}{2}g^2\right)\lambda_{\text{HS}}, \quad (\text{B2})
\end{aligned}$$

$$16\pi^2\beta_{\lambda_S} = 18\lambda_S^2 + 2\lambda_{\text{HS}}^2, \quad (\text{B3})$$

$$16\pi^2\beta_g = -\frac{19}{6}g^3. \quad (\text{B4})$$

$$16\pi^2\beta_{g'} = \frac{41}{6}g^3, \quad (\text{B5})$$

$$16\pi^2\beta_{g_s} = -7g_s^3, \quad (\text{B6})$$

TABLE I. The critical temperature of the electroweak phase transition (T_c) and the Higgs VEV (v_c) for different values of the renormalization scale.

μ_R (GeV)	T_c (GeV)	v_c (GeV)
86.5	148.987	30
173.0	148.326	23
246.2	148.002	20
346.0	147.693	18

$$16\pi^2\beta_{y_i} = \frac{9}{2}y_i^3 - \left(\frac{9}{4}g^2 + \frac{17}{12}g^2 + 8g_s^2\right)y_i, \quad (\text{B7})$$

where the one-loop beta function is defined as

$$\beta_g = \mu \frac{dg}{d\mu}. \quad (\text{B8})$$

-
- [1] K. N. Abazajian *et al.* (CMB-S4 Collaboration), [arXiv:1610.02743](#).
- [2] M. H. Abitbol *et al.* (Simons Observatory Collaboration), *Bull. Am. Astron. Soc.* **51**, 147 (2019).
- [3] S. Hild, M. Abernathy, F. Acernese, P. Amaro-Seoane, N. Andersson, K. Arun, F. Barone, B. Barr, M. Barsuglia, M. Beker *et al.*, *Classical Quantum Gravity* **28**, 094013 (2011).
- [4] J. Baker, J. Bellovary, P. L. Bender, E. Berti, R. Caldwell, J. Camp, J. W. Conklin, N. Cornish, C. Cutler, R. DeRosa *et al.*, [arXiv:1907.06482](#).
- [5] T. L. Smith and R. Caldwell, *Phys. Rev. D* **100**, 104055 (2019).
- [6] J. Crowder and N. J. Cornish, *Phys. Rev. D* **72**, 083005 (2005).
- [7] T. L. Smith and R. Caldwell, *Phys. Rev. D* **95**, 044036 (2017).
- [8] N. Seto, S. Kawamura, and T. Nakamura, *Phys. Rev. Lett.* **87**, 221103 (2001).
- [9] S. Kawamura, M. Ando, N. Seto, S. Sato, M. Musha, I. Kawano, J. Yokoyama, T. Tanaka, K. Ioka, T. Akutsu *et al.*, *Prog. Theor. Exp. Phys.* **2021**, 05A105 (2021).
- [10] A. Weltman, P. Bull, S. Camera, K. Kelley, H. Padmanabhan, J. Pritchard, A. Raccanelli, S. Riemer-Sørensen, L. Shao, S. Andrianomena *et al.*, *Publ. Astron. Soc. Aust.* **37**, e002 (2020).
- [11] P. Auclair *et al.* (LISA Cosmology Working Group), *Living Rev. Relativity* **26**, 5 (2023).
- [12] G. Agazie *et al.* (NANOGrav Collaboration), *Astrophys. J. Lett.* **951**, L8 (2023).
- [13] J. Antoniadis, P. Arumugam, S. Arumugam, S. Babak, M. Bagchi, A. S. B. Nielsen, C. G. Bassa, A. Bathula, A. Berthereau, M. Bonetti *et al.*, *Astron. Astrophys.* **678**, A50 (2023).
- [14] D. J. Reardon, A. Zic, R. M. Shannon, G. B. Hobbs, M. Bailes, V. Di Marco, A. Kapur, A. F. Rogers, E. Thrane, J. Askew *et al.*, *Astrophys. J. Lett.* **951**, L6 (2023).
- [15] H. Xu, S. Chen, Y. Guo, J. Jiang, B. Wang, J. Xu, Z. Xue, R. N. Caballero, J. Yuan, Y. Xu *et al.*, *Res. Astron. Astrophys.* **23**, 075024 (2023).
- [16] M. E. Carrington, *Phys. Rev. D* **45**, 2933 (1992).
- [17] K. Kajantie, M. Laine, K. Rummukainen, and M. E. Shaposhnikov, *Nucl. Phys.* **B466**, 189 (1996).
- [18] C. E. M. Wagner, *Lett. High Energy Phys.* **2023**, 466 (2023).
- [19] M. Laine, G. Nardini, and K. Rummukainen, *J. Cosmol. Astropart. Phys.* **01** (2013) 011.
- [20] A. D. Sakharov, *Pis'ma Zh. Eksp. Teor. Fiz.* **5**, 32 (1967).
- [21] R. Apreda, M. Maggiore, A. Nicolis, and A. Riotto, *Nucl. Phys.* **B631**, 342 (2002).
- [22] R. M. Schabinger and J. D. Wells, *Phys. Rev. D* **72**, 093007 (2005).
- [23] A. Kusenko, *Phys. Rev. Lett.* **97**, 241301 (2006).
- [24] J. McDonald, *Phys. Rev. D* **50**, 3637 (1994).
- [25] M. Chala, C. Krause, and G. Nardini, *J. High Energy Phys.* **07** (2018) 062.
- [26] H. Davoudiasl, R. Kitano, T. Li, and H. Murayama, *Phys. Lett. B* **609**, 117 (2005).
- [27] I. Baldes, T. Konstandin, and G. Servant, *Phys. Lett. B* **786**, 373 (2018).
- [28] A. Noble and M. Perelstein, *Phys. Rev. D* **78**, 063518 (2008).
- [29] R. Zhou, J. Yang, and L. Bian, *J. High Energy Phys.* **04** (2020) 071.
- [30] D. J. Weir, *Phil. Trans. R. Soc. A* **376**, 20170126 (2018).
- [31] M. B. Hindmarsh, M. Lüben, J. Lumma, and M. Pauly, *SciPost Phys. Lect. Notes* **24**, 1 (2021).
- [32] X. F. Han, L. Wang, and Y. Zhang, *Phys. Rev. D* **103**, 035012 (2021).
- [33] H. L. Child and J. T. Giblin, Jr., *J. Cosmol. Astropart. Phys.* **10** (2012) 001.
- [34] M. Fairbairn and R. Hogan, *J. High Energy Phys.* **09** (2013) 022.
- [35] C. Caprini, M. Hindmarsh, S. Huber, T. Konstandin, J. Kozaczuk, G. Nardini, J. M. No, A. Petiteau, P. Schwaller, G. Servant *et al.*, *J. Cosmol. Astropart. Phys.* **04** (2016) 001.
- [36] S. J. Huber, T. Konstandin, G. Nardini, and I. Rues, *J. Cosmol. Astropart. Phys.* **03** (2016) 036.
- [37] C. Delaunay, C. Grojean, and J. D. Wells, *J. High Energy Phys.* **04** (2008) 029.
- [38] D. J. H. Chung, A. J. Long, and L. T. Wang, *Phys. Rev. D* **87**, 023509 (2013).
- [39] G. Barenboim and J. Rasero, *J. High Energy Phys.* **07** (2012) 028.
- [40] E. Senaha, *Symmetry* **12**, 733 (2020).
- [41] C. Grojean and G. Servant, *Phys. Rev. D* **75**, 043507 (2007).
- [42] A. Katz and M. Perelstein, *J. High Energy Phys.* **07** (2014) 108.

- [43] A. Alves, T. Ghosh, H. K. Guo, K. Sinha, and D. Vagie, *J. High Energy Phys.* **04** (2019) 052.
- [44] P. Athron, C. Balázs, A. Fowlie, L. Morris, and L. Wu, *Prog. Part. Nucl. Phys.* **135**, 104094 (2024).
- [45] S. Profumo, M. J. Ramsey-Musolf, and G. Shaughnessy, *J. High Energy Phys.* **08** (2007) 010.
- [46] P. H. Damgaard, D. O'Connell, T. C. Petersen, and A. Tranberg, *Phys. Rev. Lett.* **111**, 221804 (2013).
- [47] A. Ashoorioon and T. Konstandin, *J. High Energy Phys.* **07** (2009) 086.
- [48] D. O'Connell, M. J. Ramsey-Musolf, and M. B. Wise, *Phys. Rev. D* **75**, 037701 (2007).
- [49] J. M. Cline and K. Kainulainen, *J. Cosmol. Astropart. Phys.* **01** (2013) 012.
- [50] M. Gonderinger, H. Lim, and M. J. Ramsey-Musolf, *Phys. Rev. D* **86**, 043511 (2012).
- [51] S. Profumo, L. Ubaldi, and C. Wainwright, *Phys. Rev. D* **82**, 123514 (2010).
- [52] M. Gonderinger, Y. Li, H. Patel, and M. J. Ramsey-Musolf, *J. High Energy Phys.* **01** (2010) 053.
- [53] V. Barger, P. Langacker, M. McCaskey, M. Ramsey-Musolf, and G. Shaughnessy, *Phys. Rev. D* **79**, 015018 (2009).
- [54] C. Cheung, M. Papucci, and K. M. Zurek, *J. High Energy Phys.* **07** (2012) 105.
- [55] T. Alanne, K. Tuominen, and V. Vaskonen, *Nucl. Phys.* **B889**, 692 (2014).
- [56] J. R. Espinosa, T. Konstandin, and F. Riva, *Nucl. Phys.* **B854**, 592 (2012).
- [57] J. R. Espinosa and M. Quiros, *Phys. Rev. D* **76**, 076004 (2007).
- [58] V. Barger, P. Langacker, M. McCaskey, M. J. Ramsey-Musolf, and G. Shaughnessy, *Phys. Rev. D* **77**, 035005 (2008).
- [59] J. M. Cline, K. Kainulainen, P. Scott, and C. Weniger, *Phys. Rev. D* **88**, 055025 (2013); **92**, 039906(E) (2015).
- [60] C. P. Burgess, M. Pospelov, and T. ter Veldhuis, *Nucl. Phys.* **B619**, 709 (2001).
- [61] M. Kakizaki, S. Kanemura, and T. Matsui, *Phys. Rev. D* **92**, 115007 (2015).
- [62] K. Enqvist, S. Nurmi, T. Tenkanen, and K. Tuominen, *J. Cosmol. Astropart. Phys.* **08** (2014) 035.
- [63] J. R. Espinosa and M. Quiros, *Phys. Lett. B* **305**, 98 (1993).
- [64] A. Beniwal, M. Lewicki, J. D. Wells, M. White, and A. G. Williams, *J. High Energy Phys.* **08** (2017) 108.
- [65] D. Curtin, P. Meade, and C. T. Yu, *J. High Energy Phys.* **11** (2014) 127.
- [66] C. W. Chiang, Y. T. Li, and E. Senaha, *Phys. Lett. B* **789**, 154 (2019).
- [67] P. S. B. Dev, F. Ferrer, Y. Zhang, and Y. Zhang, *J. Cosmol. Astropart. Phys.* **11** (2019) 006.
- [68] K. Ghorbani and P. H. Ghorbani, *J. Phys. G* **47**, 015201 (2020).
- [69] P. Ghorbani, *Phys. Dark Universe* **33**, 100861 (2021).
- [70] G. Kurup and M. Perelstein, *Phys. Rev. D* **96**, 015036 (2017).
- [71] S. R. Coleman and E. J. Weinberg, *Phys. Rev. D* **7**, 1888 (1973).
- [72] P. Athron, C. Balazs, A. Fowlie, L. Morris, G. White, and Y. Zhang, *J. High Energy Phys.* **01** (2023) 050.
- [73] D. Croon, O. Gould, P. Schicho, T. V. I. Tenkanen, and G. White, *J. High Energy Phys.* **04** (2021) 055.
- [74] O. Gould and T. V. I. Tenkanen, *J. High Energy Phys.* **06** (2021) 069.
- [75] S. P. Martin, *Phys. Rev. D* **90**, 016013 (2014).
- [76] J. Elias-Miro, J. R. Espinosa, and T. Konstandin, *J. High Energy Phys.* **08** (2014) 034.
- [77] A. Andreassen, W. Frost, and M. D. Schwartz, *Phys. Rev. D* **91**, 016009 (2015).
- [78] A. Andreassen, W. Frost, and M. D. Schwartz, *Phys. Rev. Lett.* **113**, 241801 (2014).
- [79] M. Bando, T. Kugo, N. Maekawa, and H. Nakano, *Phys. Lett. B* **301**, 83 (1993).
- [80] C. Tamarit, *Phys. Rev. D* **90**, 055024 (2014).
- [81] M. Quiros, [arXiv:hep-ph/9901312](https://arxiv.org/abs/hep-ph/9901312).
- [82] M. Laine and A. Vuorinen, *Lect. Notes Phys.* **925**, 1 (2016).
- [83] G. W. Anderson and L. J. Hall, *Phys. Rev. D* **45**, 2685 (1992).
- [84] D. Curtin, P. Meade, and H. Ramani, *Eur. Phys. J. C* **78**, 787 (2018).
- [85] R. R. Parwani, *Phys. Rev. D* **45**, 4695 (1992); **48**, 5965(E) (1993).
- [86] P. B. Arnold and O. Espinosa, *Phys. Rev. D* **47**, 3546 (1993); **50**, 6662(E) (1994).
- [87] E. J. Weinberg and A. q. Wu, *Phys. Rev. D* **36**, 2474 (1987).
- [88] M. Trodden, *Rev. Mod. Phys.* **71**, 1463 (1999).
- [89] A. Riotto, [arXiv:hep-ph/9807454](https://arxiv.org/abs/hep-ph/9807454).
- [90] A. Riotto and M. Trodden, *Annu. Rev. Nucl. Part. Sci.* **49**, 35 (1999).
- [91] D. E. Morrissey and M. J. Ramsey-Musolf, *New J. Phys.* **14**, 125003 (2012).
- [92] A. G. Cohen, D. B. Kaplan, and A. E. Nelson, *Annu. Rev. Nucl. Part. Sci.* **43**, 27 (1993).
- [93] H. H. Patel and M. J. Ramsey-Musolf, *J. High Energy Phys.* **07** (2011) 029.
- [94] K. Fuyuto and E. Senaha, *Phys. Rev. D* **90**, 015015 (2014).
- [95] V. Vaskonen, *Phys. Rev. D* **95**, 123515 (2017).
- [96] F. P. Huang, Z. Qian, and M. Zhang, *Phys. Rev. D* **98**, 015014 (2018).
- [97] M. Jiang, L. Bian, W. Huang, and J. Shu, *Phys. Rev. D* **93**, 065032 (2016).
- [98] B. Grzadkowski and D. Huang, *J. High Energy Phys.* **08** (2018) 135.
- [99] J. M. Cline, K. Kainulainen, and A. P. Vischer, *Phys. Rev. D* **54**, 2451 (1996).
- [100] J. R. Espinosa, B. Gripaios, T. Konstandin, and F. Riva, *J. Cosmol. Astropart. Phys.* **01** (2012) 012.
- [101] B. Jain, S. J. Lee, and M. Son, *Phys. Rev. D* **98**, 075002 (2018).
- [102] P. Athron *et al.* (GAMBIT Collaboration), *Eur. Phys. J. C* **77**, 568 (2017).
- [103] P. Athron, J. M. Cornell, F. Kahlhoefer, J. McKay, P. Scott, and S. Wild, *Eur. Phys. J. C* **78**, 830 (2018).
- [104] L. Feng, S. Profumo, and L. Ubaldi, *J. High Energy Phys.* **03** (2015) 045.

- [105] ATLAS Collaboration, Combination of searches for invisible Higgs boson decays with the ATLAS experiment, Report No. ATLAS-CONF-2020-052, CERN.
- [106] A. M. Sirunyan *et al.* (CMS Collaboration), *Phys. Lett. B* **793**, 520 (2019).
- [107] R. L. Workman *et al.* (Particle Data Group), *Prog. Theor. Exp. Phys.* **2022**, 083C01 (2022).
- [108] ATLAS Collaboration, *Phys. Lett. B* **842**, 137963 (2023).
- [109] Y. B. Zeldovich, I. Y. Kobzarev, and L. B. Okun, *Zh. Eksp. Teor. Fiz.* **67**, 3 (1974).
- [110] A. Angelescu, F. Goertz, and A. Tada, *J. High Energy Phys.* **10** (2022) 019.
- [111] M. Dine, R. G. Leigh, P. Y. Huet, A. D. Linde, and D. A. Linde, *Phys. Rev. D* **46**, 550 (1992).
- [112] L. Dolan and R. Jackiw, *Phys. Rev. D* **9**, 3320 (1974).
- [113] M. Gürtler, E. M. Ilgenfritz, and A. Schiller, *Phys. Rev. D* **56**, 3888 (1997).
- [114] M. Laine and K. Rummukainen, *Nucl. Phys. B, Proc. Suppl.* **73**, 180 (1999).
- [115] F. Csikor, Z. Fodor, and J. Heitger, *Phys. Rev. Lett.* **82**, 21 (1999).
- [116] Y. Aoki, F. Csikor, Z. Fodor, and A. Ukawa, *Phys. Rev. D* **60**, 013001 (1999).